NASA CONTRACTOR REPORT

NASA CR-62025

NASA CR-62025

OPERATIONAL APPLICATION OF A UNIVERSAL TURBULENCE MEASURING SYSTEM

Prepared Under Contract NAS4-784 by

Paul B. MacCready, Jr., Robin E. Williamson,
Stephen Berman, and Alexander Webster

METEOROLOGY RESEARCH, INC.
Altadena, California

For

NASA - FLIGHT RESEARCH CENTER
Edwards, Calif.

November 1965

NASA CR-62025

OPERATIONAL APPLICATION OF A UNIVERSAL TURBULENCE MEASURING SYSTEM

by

Paul B. MacCready, Jr.
Robin E. Williamson
Stephen Berman
Alexander Webster

Prepared under Contract No. NAS4-784

METEOROLOGY RESEARCH, INC.
2420 North Lake Avenue
Altadena, California

for

NATIONAL AERONAUTICS AND SPACE ADMINISTRATION
Flight Research Center
Edwards, California

FOREWORD

This report presents the final results of a limited program of study, development and tests conducted by Meteorology Research, Incorporated under NASA Contract NAS 4-784 with the NASA Flight Research Center at Edwards AFB, California. The NASA project monitor was Mr. Jack Ehrenberger; Dr. Paul B. MacCready, Jr., was the principal investigator.

The fundamental concepts on which the universal turbulence system is based, here reviewed in Appendix A, have been previously reported by MacCready; Mr. E. Phillips provided the basic design of the optimum circuitry described in Appendix B; the alternate circuitry and analysis in Appendix B was supplied by Dr. J. H. Marshall of Analog Technology Corporation; most of the aircraft response and human factors discussion in Appendix C was developed by Mr. Robert Stapleford of Systems Technology, Incorporated.

This report concludes Contract NAS 4-784.

TABLE OF CONTENTS

LIST OF TABLES

LIST OF FIGURES

OPERATIONAL APPLICATION OF A UNIVERSAL TURBULENCE MEASURING SYSTEM

by

Paul B. MacCready, Jr.
Robin E. Williamson
Stephan Berman
Alexander Webster

SUMMARY

A multi-phased program was conducted to advance the universal turbulence measurement concept toward operational status. The concept is based on the fact that there are simplifications in statistical turbulence relationships when concern is with the relatively small wavelengths which put the major gust loads on aircraft. A simple system called the Universal Indicated Turbulence System (UITS) gives an output reading R which is a quantitative measure of turbulence intensity unaffected by the characteristics or speed of the aircraft on which it is mounted. The UITS utilizes a high frequency dynamic pressure sensor. Various versions of the associated electronic circuitry were designed and analyzed, and an optimum design established.

Theoretical studies have developed the relation between R and the RMS gust loads on the aircraft (σ_g; i.e., $\sigma_g \sim (\text{IAS}) \times R$, where IAS is indicated airspeed and the constant of proportionality depends only on the aircraft wing loading and lift curve slope. The constant was determined for various types of aircraft. The assumption that the human evaluation of turbulent severity, σ_h, is dependent on the energy encountered at particular frequencies results in $\sigma_h \sim (\text{IAS})^{4/3} R$. Considering the order of subjective accuracy required here, σ_h can be taken as proportional to σ_g since the exponents of the IAS terms are close.

An intensity scale for R is suggested with a corresponding scale for σ_g (or σ_h). Both scales are in agreement at a specific speed for each aircraft.

A UITS prototype was operationally tested in a T-33 aircraft demonstrating an all-weather capability. R indications and the observer's turbulence evaluations were reasonably consistent with the theoretical predictions. An Apache aircraft was instrumented for complete two-component, turbulence measurements. An estimate of the best averaging time for the UITS reading was obtained by analyzing the data from the Apache for the time histories of the power spectral density components and also by playing the Apache magnetic tape record into the final UITS circuitry.

INTRODUCTION

The project aim is to develop and verify a technique which permits an air turbulence measurement by a relatively simple system for installation in operational aircraft. The air turbulence measurement is standardized and independent of aircraft response and crew performance. That is, a measurement is made of the local statistical turbulent property of the air rather than anything dependent upon the measuring device. The intensity measure can be used to predict quantitatively the effect of turbulence on specific aircraft in specific flight modes.

To advance the Universal Turbulence System toward a truly operational status requires development effort in three related areas. The first area is in providing a sensor compatible with the all-weather operations of subsonic aircraft. The second area relates to providing an overall electronic system featuring appropriate simplicity and reliability. Finally there is involved establishing the quantitative relationships between the instrument reading and the statistical gust loads on aircraft, or the instrument reading and the assessment of discomfort by pilot or passengers. The flight test of a prototype air turbulence measuring system, a detailed study to determine the optimum system parameters, analysis of the flight performance, and suggestions for an optimum instrument and its use are covered in this report.

The Universal Turbulence System is based on the concepts (ref. 1) that: (a) the main contribution to the gust loads on an aircraft and to the human "feel" of turbulence effects arises from turbulent eddies in a size range where the statistical properties of the natural turbulence are particularly simple; (b) the intensity of the turbulence in this eddy size range can be designated by a quantity $\epsilon^{1/3}$ which can be measured simply on an aircraft no matter what the speed of the aircraft is or what type of aircraft is involved; and (c) with knowledge of the aircraft response, the average gust loads and the human feel of turbulence can be related to $\epsilon^{1/3}$. These concepts lead to the use of $\epsilon^{1/3}$ as the basis of a standard measurement of turbulence intensity.

Prior system studies and analysis by the contractor had established that a pressure pickup would be a suitable sensor for an operational system. Originally a fast-response propeller sensor was used in the Universal Turbulence Indicator (UTI). The present scheme based on a pressure sensor has been labeled the Universal Indicated Turbulence System (UITS) since it has a density factor included in its reading. The UITS output reading, R, is $(\rho\epsilon/\rho_0)^{1/3}$. R represents a universal turbulence quantity since the same value would be indicated on the UITS output from any subsonic aircraft flying at any airspeed through a particular region of turbulence.

SYMBOLS

B	$(gSC_{L_\alpha})/(2\ W)$
C_s	a dimensionless constant (empirical) = 0.15
C_{L_α}	Slope of the lift curve, $dC_L/d\alpha$, where C_L is the lift coefficient and α is the angle-of-attack Note: $C_{L_\alpha} = 2\pi$ for a wing of high aspect ratio
E(f) E(k)	Power spectral density of the u component (twice the energy per unit mass per unit wave number or frequency) $\overline{w^2} = \int_0^\infty E(k)\ dk$
f	Frequency (= Uk), cycles/time
G(f) G(k)	Power spectral density of the w component $G(k) = \frac{4}{3} E(k)$, for isotropic turbulence having spectra $\sim k^{-5/3}$
IAS	Indicated airspeed ($= \sqrt{\rho/\rho_0}\ U$)
J(f)	Power spectral density of fluctuating voltage m
K	knots
k	Wave Number, cycles/length
M	Voltage out of pressure transducer ($\sim \Delta p$)
M_o	Mean value of M
m	Fluctuating part of M
N	A voltage
N_o	Mean value of N
n	Fluctuating part of N
Δp	= total pressure - static pressure
q	$= \frac{1}{2} \rho U^2$ (incompressible)
R	$= (\rho \epsilon/\rho_0)^{1/3}$ - output of the UITS, length $^{2/3}$/time
S	Aircraft wing area
U	True airspeed ($= U_0 + u$)

UITS	Universal Indicated Turbulence System
u	Component of the true turbulent velocity parallel to the flight path
W	Aircraft weight
w	Component of the true turbulent velocity normal (up) to flight path
$\ddot{z}$	Vertical acceleration
ϵ	Dissipation rate, length^2/time^3. $\epsilon^{1/3}$ can be considered a turbulence intensity measure
λ	Wavelength, length/cycle ($=k^{-1}$)
ρ	Air density, mass/length^3
ρ_o	Sea level air density
σ_g	RMS of vertical acceleration in "g" units, length/time^2
σ_h	Personal estimate of intensity of turbulence effect on an aircraft
τ	Circuit time constant
ω	Angular frequency, radians/time ($=2\pi f$)

RESULTS

The details of the studies and results are given in the individual appendices. The main points are summarized here.

A. System Design

1. The Transducers

The UITS presented here is based on a fast response differential pressure pickup. This transducer provides the turbulence fluctuation signal and also the mean-level signal needed to control the gain of the fluctuating voltage. In Appendix B it is pointed out that with the same system electronics an accelerometer can be substituted as the source of the turbulence fluctuation signal, although this method has some disadvantages when compared to the standard UITS approach.

2. Methods of Gain Control of the Fluctuating Voltages

Mechanical (nonlinear pressure diaphragm constraint): deemed far too critical and complex in actual production.

Servo System: straightforward, to be used in case alternative systems prove impractical, but more expensive and potentially less reliable than desired.

Raysistor Reciprocal Gain Controlled Amplifier: the best method of the ones investigated. This one has been completely breadboarded and tested with a magnetic-taped turbulence signal.

Quadratron Exponential Resistor Cube Root Amplifier: too complex and temperature sensitive for operational application.

Silicon Diode Gain Controlled Amplifier:
Silicon Diode Cube Root Amplifier:
Cube Root System Using Averaging:
Cube Root System Using Peak Detection:
} promising, but not evaluated in detail

Thus, of the various ways to accomplish the gain variation with pressure (speed), the recommended method involves using a Raysistor in a reciprocal gain circuit. Nonlinearities in the circuit make the gain vary as $M_0^{-2/3}$ rather than the reciprocal M_0^{-1}.

3. Filter Considerations

A passive filter is adequate for the UITS, and far simpler than an active one. Based on test results, the averaging time for an operational instrument appears to be about 6 to 10 seconds, with shorter averaging for research purposes or high speed jet aircraft. A block diagram of the optimum system is given on Fig. B12.

B. Aircraft and Human Response

1. Relation Between σ_g and R for -5/3 Spectrum

The relation between R and RMS gust load, σ_g, is, for a rigid, non-pitching aircraft in turbulence having a -5/3 spectrum:

$$\sigma_g = 1.46 \cdot 10^{-2} \left(\frac{W}{S C_{L_\alpha}}\right)^{-2/3} \cdot IAS \cdot R \cdot \left(\frac{\rho}{\rho_o}\right)^{-1/6} \qquad (1)$$

for σ_g in g units, $W/S C_{L_\alpha}$ in lb ft^{-2}, IAS in knots, R in m$^{2/3}$sec^{-1}.[1] The constant is $6.8 \cdot 10^{-4}$ if R is in cm$^{2/3}$sec^{-1}.

Because the exponent of the density effect is small, the density factor from 0 to 40,000 ft varies only ±10 per cent from the intermediate value at, say, 20,000 ft. Thus if $(\rho/\rho_o)^{1/6}$ is taken as a constant, equalling 0.9, Eq. (1) becomes,

$$\sigma_g = \left[7.5 \cdot 10^{-4}\right] \left(\frac{W}{S C_{L_\alpha}}\right)^{-2/3} \cdot IAS \cdot R \qquad (2)$$

2. Relation Between σ_g and R for Two-Piece Combined Spectrum

A different turbulent spectrum shape can more realistically cover a broad wavelength range, namely the -5/3 law to a specific wave number k_1 and flat for all smaller wave numbers. Using this spectrum, then

$$\sigma_g = \left(\text{function of } \frac{W}{S C_{L_\alpha}},\ \rho,\ k_1\right) \cdot IAS \cdot R \qquad (3)$$

Taking representative aircraft types, altitudes, and loadings, one finds that for $k_1 = (2000 \text{ ft})^{-1}$ the density effect in the term in parentheses practically vanishes. Thus, for practical purposes,

$$\sigma_g = \left(\text{function of } \frac{W}{S C_{L_\alpha}}\right) \cdot IAS \cdot R \qquad (4)$$

[1] The mixed units were chosen as being the most conventional for the particular quantities involved.

By fitting a simple curve to the empirical data of Fig. C2, p C-11,

$$\sigma_g = \left[7.5 \times 10^{-4}(1 - 0.111x + 0.0077x^2)\right]\left[\frac{W}{S C_{L_\alpha}}\right]^{-2/3} IAS \times R \qquad (5)$$

where

$$x = \frac{W}{S C_{L_\alpha}} \times \frac{4\pi k_1}{g \rho_{20\,000\,ft}} \qquad (6)$$

with g in ft/sec^2 and ρ in slugs/ft^3.

Table 1 gives representative values of the constants in Eqs. (2) and (4) for a range of typical aircraft, as adapted from Table C1 in Appendix C. They are presented in terms of σ_g in g units, IAS in knots, and R in c m$^{2/3}$sec^{-1}

$$\sigma_g = \left[\text{const.}\right]\frac{IAS}{100} \times R \qquad (7)$$

Table 1

RESPONSE FUNCTIONS FOR VARIOUS AIRCRAFT

Aircraft	For $k_1 = \infty$ [const.]	For $k_1 = (2000\ ft)^{-1}$ [const.]
Cessna 180	0.0342	0.0328
Beech 65-90	0.0232	0.0211
T-33A	0.0180	0.0156
707-420 at 180,000 lbs	0.0120	0.0093
707-420 at 280,000 lbs	0.0089	0.0062

The difference between the first and second columns gives evidence of how much contribution to σ_g arises from wavelengths beyond 2000 ft. For the lightly loaded Cessna 180, the difference is negligible, while the effect is large for the heavily loaded Boeing 707.

3. Validity of the Concept

The ratio of σ_g/R will be (const.) $\times$ IAS if the inertial subrange concept is perfectly valid. To check the actual degree of validity, one can note the G(f) energy in the 200 - 2000 ft. wavelength range which contributed most to σ_g for typical operational aircraft, and the E(f) energy in the 20 to 200 ft. range which contributes most to R. Spectra curves for CAT measured at constant airspeed taken from reference 2, shown in Appendix E, were examined for the particular ratio G/E. The square root of this quantity is proportional to σ_g/R for a given airspeed. Normalizing the square root

ratios to a mean value of unity and deleting the two extreme cases, the 5 values are 0.98, 0.87, 1.09, 1.04, and 1.00. Further substantiation of the ratio $\sigma_g/(R \times IAS)$ being constant is given for the T-33 data in Appendix D.

4. Relationships Between σ_h and σ_g.

There is no known exact relation between aircraft accelerations and the feel of turbulence severity as described by pilots, crew, or passengers. However, studies cited in Appendix C suggest that the human feel (call it σ_h) depends mostly on the acceleration in particular frequency bands (especially around 1 cps and 5 cps) rather than on the total σ_g. The derivation of the σ_h vs. R relationship is simplified because, in any aircraft, all of the frequencies of concern presumably relate to the inertial subrange. Whatever the exact contributions to σ_h are, so long as the effect depends on the energies at particular frequencies or frequency bands the σ_h vs R relationship turn out to be

$$\sigma_h \sim \left[\frac{W}{S C_{L_\alpha}}\right]^1 (IAS)^{4/3} R \qquad (8)$$

Thus, σ_g and σ_h are not strictly proportional, since for a given turbulence the former varies as $(IAS)^1$ while the latter as $(IAS)^{4/3}$. The difference is fortunately not very large. For example, if σ_g and σ_h are matched at 200 K, the difference at 130 K and 300 K is only 15 per cent.

C. Intensity Scales

1. Recommended Turbulence Intensity Scale

The recommended intensity scale of turbulence is a function of R. For the scale, the following values are recommended. They have the relative ratio suggested by ref. 1, with the scale adjusted for the best compromise with the data available in refs. 2 and 3, Appendix E, and considerations from Appendix D.

Table 2

RECOMMENDED TURBULENCE SCALE

Magnitude	Descriptive Title	$R \sim cm^{2/3}\ sec^{-1}$
0	Negligible	< 0.8
1	Light	0.8 - 1.9
2	Moderate	1.9 - 4.5
3	Heavy	4.5 -10.7
4	Extreme	> 10.7

2. Recommended Aircraft Response and Human Description Scales

The human description of turbulence, σ_h, is not identical to σ_g but can be considered proportional to the accuracy required here. A unique scale can thus be established relating σ_g to a pilot-derived aircraft response scale. Such a scale (see Table 3, below) follows the intensity descriptions and ratios of Table 2 with the values scaled to agree essentially with the results of ref. 3.

Table 3

AIRCRAFT RESPONSE AND HUMAN DESCRIPTION SCALES

Descriptive Title	σ_g in "g" units
Negligible	< 0.025
Light	0.025 - 0.06
Moderate	0.06 - 0.15
Heavy	0.15 - 0.34
Extreme	> 0.34

Thus σ_g has the same description or title as the turbulence scale R for a particular IAS for each aircraft (call this IAS_c). This can be seen by comparing the two scale lists and utilizing Eq. (7) with the constants derived for $k_1 = (2000 \text{ ft})^{-1}$.

Table 4

EQUIVALENT AIR SPEED FOR SELECTED AIRCRAFT

Aircraft	IAS_c - Knots
Cessna 180	98
Beech 65-90	123
T-33A	165
707-420 at 180,000 lbs	278
707-420 at 280,000 lbs	417

3. Other Intensity Factors

The intensity scale of the response to turbulence depends on the particular relationship being considered.

For purposes of average gust loads, σ_g is the criterion. In steady state turbulence, where structural failure can result from peak aerodynamic loads, the extreme values should also statistically relate to σ_g.

For purposes of human discomfort to turbulence, the quantity σ_h is the appropriate criterion.

For the problem of structural fatigue, some other quantity may be most appropriate. If the structural fatigue can be related primarily to the energy at particular frequencies, then the quantity giving its magnitude would be proportional to σ_h .

For other flight modes, such as aiming accuracy, formation flying, and coordination during aerial refueling, appropriate criteria would be established. If the factor is related primarily to effects in the inertial subrange or to just slightly larger eddies, then as with σ_g and σ_h the descriptive parameter should be linearly proportional to R.

4. Alternative Scale Criterion

Final acceptance and use of the UITS principle will depend on flight testing, in real operational situations, the final version of the instrumentation system outlined in this report. During such testing, some reassignment of labels and turbulence intensity and response intensity levels may prove desirable.

D. Operational Considerations

The data presentation scheme with the UITS depends on the particular application. For general communication about turbulence intensity, the turbulence level must be shown as an indicator needle position, a number on a chart, etc. Either the R reading or the turbulence scale labels suggested previously under H can be used. For research projects probably R is the better, while for operational use and communications probably the intensity scales are more appropriate. It would be desirable if some of the data communication could be made fully automatic. For example, the turbulence quantity (whenever the level is #2, moderate, #3, heavy, or #4, extreme) could be telemetered automatically from all aircraft to FAA radar stations as altitude is being done. This would provide real time plots of the distribution of regions of high turbulence, for purposes of flight planning.

In an individual aircraft, it would be desirable for the pilot to be able to predict, simply, the sort of turbulent effect he could expect on the aircraft when he reaches the area having a specified R value. This information is given by Eq. (7). R and IAS are involved, but fortunately not density. Obviously on a small card the σ_g versus R or σ_h versus R for various air speed ranges could be compiled for the particular aircraft type. It

would be more convenient to integrate the card into the R indicator on the aircraft so that, by a small adjustment knob which selects the IAS of interest, the aircraft response would be set next to the R scale. Ordinarily, since aircraft spend most of their time in a fairly narrow IAS range, the adjustment would be left fixed and only altered if, for expected heavy or extreme turbulence, the pilot wished to establish what speed is comfortable or safe.

November 1965
Meteorology Research, Inc.
Altadena, California

REFERENCES

1. MacCready, P. B., Jr.: Standardization of Gustiness Values from Aircraft. J. of Appl. Meteor., vol. 3, no. 4, 1964, pp 439-449.

2. Reiter, E. R. and Burns, A.: Atmospheric Structure and Clear Air Turbulence. Colorado State Univ., Atmos. Science Tech. Paper No. 65, June, 1965.

3. Zbrozek, J. K.: Aircraft and Atmospheric Turbulence. Royal Air. Estab. Tech. Note No. AERO 2790, 1961.

4. Kendall, James: Time-Lags Due to Compressible Poiseuille Flow Resistance in Pressure Measuring Systems. M. S. Thesis (Physics), Univ. of Maryland, 1950.

5. Stuart, J. L.: Solid State Logarithmic Amplifier. Jet Propulsion Laboratory, Space Program Summary 37-18, vol. IV, Dec. 1962.

6. Dieterich, F. W.: The Planform Parameter for Correlating Certain Aerodynamic Characteristics of Swept Wings. NACA TN 2335, 1951.

7. Parks, D. L., and F. W. Snyder: Human Reaction to Low Frequency Vibration. Doc. No. D3-3512-1, The Boeing Co., Wichita Div., July, 1961.

8. Computers Using Statistical and Regression Techniques. Bull. No. ALAC 62023, Electronics Assoc., Inc., 1964.

APPENDIX A

BASIC FACTORS IN THE UNIVERSAL TURBULENCE SYSTEM

The following items from the conclusions of ref. 1 summarize the main factors involved in the universal turbulence measurement and the application of the measurement to operational problems. The present report is based on the considerations given below. It clarifies and makes quantitative many relationships, particularly the altitude and airspeed effects on the σ_g vs $\epsilon^{1/3}$ and the σ_h vs $\epsilon^{1/3}$ dependence.

1) It is operationally desirable to have a measure of turbulence intensity which relates to the atmospheric turbulence itself instead of to its effect on aircraft.

2) The inertial subrange concept relates all the statistical quantities of eddies in its size range to a single quantity, ϵ, an "energy dissipation" factor. The power spectrum of turbulence in any direction is proportional to $\epsilon^{2/3}\lambda^{5/3}$ where λ is the wavelength. Thus ϵ, or a function of it, provides a logical intensity factor for a turbulence standardization system.

3) The inertial subrange concept typically covers turbulence wavelengths from a few centimeters to 200 or 300 meters, and its consequences are even often reasonably valid to considerably larger wavelengths. These wavelengths related to the inertial subrange are those primarily responsible for aircraft gust loads and for some aircraft stability factors.

4) ϵ can be measured in flight with special instrumentation. The measurement can be independent of the type of aircraft or its speed. Other methods are available for ascertaining ϵ, including devices on balloons and rockets. Meteorological investigations are providing data on the distribution of ϵ in the atmosphere. Data pertaining to ϵ can also be derived from classical discrete gust studies and continuous turbulence studies, with certain assumptions about spectra and response characteristics.

5) A specific atmospheric turbulence magnitude scale is suggested, giving ranges of ϵ values to five ranges labeled "negligible, light, moderate,

heavy, extreme." The scale is based on various turbulence measurements from aircraft. (Note: The present report suggests a new scale based on $(\rho\epsilon/\rho_0)^{1/3}$ rather than $\epsilon^{1/3}$).

6) The RMS value of aircraft vertical accelerations, σ_g, is proportional to $\epsilon^{1/3}$. The constant of proportionality is different for different aircraft, aircraft weights, airspeeds, and altitudes (the variation with airspeed is greatest), but it can be computed or measured. Thus a chart can be prepared for each aircraft, showing σ_g vs $\epsilon^{1/3}$ for various speed ranges. Knowledge of ϵ will then permit the pilot to determine the airspeed to keep σ_g within desired limits. The chart can be incorporated onto the face of an ϵ-indicator. An aircraft response scale labeled "negligible, light, moderate, heavy, extreme" is given in terms of σ_g. A "standard" speed can be derived for each aircraft at which the description of aircraft response in terms of σ_g is the same as the turbulence magnitude categories in terms of ϵ.

7) The feelings of a human in turbulence are assumed to relate to σ_h, his vertical acceleration in a particular frequency band of about 2 to 8 cps with a peak of sensitivity around 3 to 5 cps. σ_h thus depends on inertial subrange gusts. The relation between σ_h and σ_g depends on the type of aircraft and its speed, but in most cases the relation should be constant enough so that σ_g can logically be used for aircraft response intensity scales. An alternative response scale can be derived based on σ_h rather than σ_g, if desired. (Note: The present report utilizes the frequency around 1 cps, and shows that the σ_h vs σ_g relationship should have a (weak) airspeed dependence).

8) The turbulence-gust load technique relates small-eddy measurements to the effects of small eddies, in contrast to the standard technique which characterizes turbulence intensity by the variance of vertical velocity. This variance is dominated by large eddies which are not so well correlated with the gust-load producing eddies. Furthermore, these eddies are difficult to measure because distinct turbulence regimes are not much larger than the eddies to be measured.

9) When acceleration loads or stability problems depend on wavelengths somewhat beyond the inertial subrange eddies, the standardization technique is still valid as long as the spectrum shape over the wavelength range of interest is constant. In this case, although the spectrum shape is not proportional to $\lambda^{5/3}$ at the long wavelengths, the energies are still uniquely related to ϵ.

10) The standardization principle requires that the vertical velocity spectrum curve have a constant shape in the wavelength range which contributes most to gust loads; additional convenient measuring techniques are available if the turbulence is isotropic; the particular scale levels selected here for turbulence magnitude descriptions are derived using inertial subrange concepts.

11) One simple technique cannot perfectly cover all situations, but the simplicity of this technique permits better coverage of varied turbulence situations and thus actually results in more quantitative usefulness than would a more complex technique.

APPENDIX B

OPTIMUM DESIGN OF THE UNIVERSAL INDICATED TURBULENCE SYSTEM

A. Systems Design - Preliminary Considerations

The Universal Turbulence System consists of an airborne sensor which produces a voltage representing a component of the atmospheric turbulence, a filter-averaging-indicating circuit which shows the apparent energy of the fluctuating voltage in a particular frequency band, and a gain-adjusting device which alters the overall sensitivity as a function of airspeed in such a manner as to make the final instrument reading independent of airspeed.

1. Sensor Selection

The transducer should accurately sense the turbulence component particularly in the range of 2-30 cps. MRI reviewed the various possibilities for a rugged, all-weather sensor covering this frequency range, and the only two genuine candidates turned out to be angle vanes (for either transverse component) and a pressure measurement of indicated airspeed (IAS). Previously for speeds below 250K a fast-response propeller was used in the Model 2007 Universal Turbulence Indicator, and one version, Model 1056 M.8 was used at higher speeds on the X-21A twin jet research aircraft. However, the propeller sensor was not suitable for all-weather work. Although the angle vane method can be made rugged, can be deiced, and can cover the needed frequency range, the additional virtues of the IAS sensor dictated the use of the latter.

Probably the most telling arguments for selection of the pressure measurement method are: (a) the IAS method senses both turbulence and airspeed with one sensor, which is convenient since both variables are needed in the Universal Turbulence System; (b) the aircraft provides a particularly stable platform for measurements of this component of turbulence, meaning the system can utilize rather long wavelengths where the energy input is high; and (c) standard pressure sensors are already established as reliable for operational aircraft. The exact location of the particular total pressure orifice is relatively unimportant; the probe can be conveniently located rather close to the aircraft skin. The static pressure probe is far more critical, but for this pickup the regular aircraft system can be used. (Long line length and low frequency response are of no concern here).

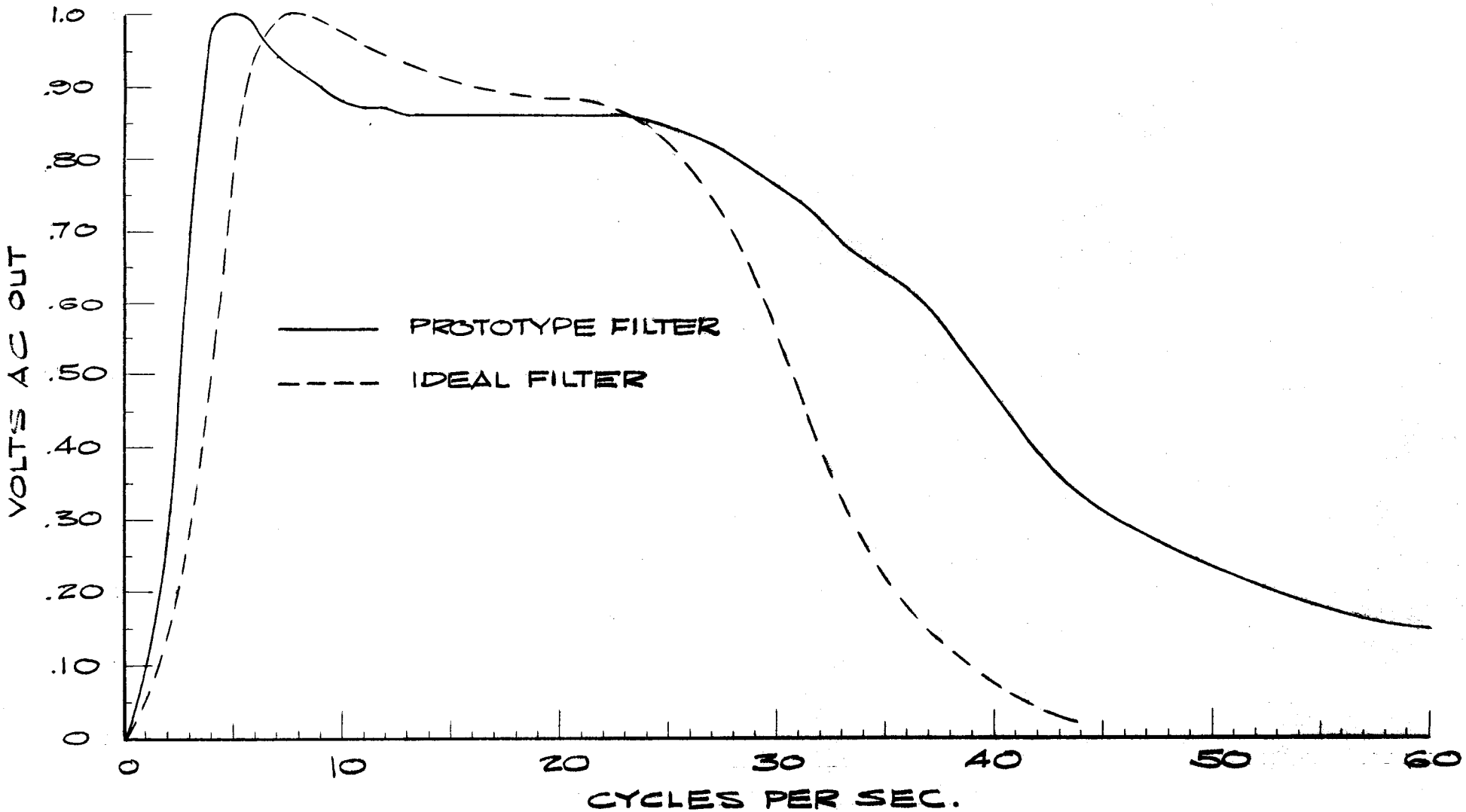

FIG. B1 IDEAL AND PROTOTYPE FILTER CHARACTERISTICS.

The subject of the length of line between the total pressure probe and the pressure transducer deserves some attention. The need for accurately handling pressure fluctuations up to 30 or 40 cps will put a limit on the line length. Calculations were made of the frequency attenuation factor for tubing I.D.'s in the $^3/_{16}$ inch range and pressure transducer geometry. Results suggest that the transducer should be rather close to the total pressure orifice, on the order of 4 to 6 ft. This means that ordinarily the transducer will not be in the cockpit, although it should be pointed out that the total pressure can be picked up effectively with a short probe well back from the aircraft nose. Thus usually the transducer will be located near the base of the total pressure probe, far from the rest of the UITS electronics. The estimates of the pressure fluctuation amplitude due to frequency were made by methods of ref. 4.

2. Filter Selection

A passive filter was selected when study showed that the desired frequency characteristics could be obtained with passive elements in an inexpensive and reasonably small package, thus permitting the system to benefit from the simplicity, stability, and reliability of the passive element approach. The particular breadboard filter was aimed at having a pass band from 4 to 20 cps, with sharp cutoffs at each end. The cutoff rate at the high frequency end is of small importance because so little energy is represented there. The exact shape in the pass band is also unimportant, although it is vital that the pass band be broad. The cutoff rate at the low frequency end is very important because the system is made most sensitive if low frequencies can be utilized, but at low frequencies around 1 or 2 cps the pilot or autopilot, rather than just the turbulence, can have some input into the turbulence measurement. Also at these same low frequencies the aircraft response may introduce errors with very light, high drag aircraft. The filter design was specified considering all these compromises.

The actual filter characteristics are shown in Fig. B1. A preferable filter characteristic is also indicated on Fig. B1. This represents a realistic filter which can be built with the same principles as the actual one, but which has a narrower pass band. The low frequency characteristics are identical to those of the existing filter but at 50 percent greater frequency, while the high frequency cutoff is given a faster dropoff than the existing one by using more stages.

3. Electronics After The Filter

The electronics following the filter are straightforward. The fluctuating signal is simply rectified and averaged. For a gaussianly distributed function the average of the rectified trace is proportional to the RMS value. Thus the

output indication will be proportional to $(\rho\epsilon/\rho_0)^{1/3}$, as derived in Appendix C. The standard electronic approach for this will subsequently be shown in Fig. B12 page B-22, which details a version of the complete final unit.

For the rest of the discussion here we will be concerned with how to alter the amplitude of the ac (turbulent) signal from the pressure transducer as a function of the mean voltage out of the pressure transducer. As derived in Appendix C the instrument will give R independent of airspeed, if the gain of the ac signal is proportional to (mean voltage)$^{-2/3}$.

4. Gain Variation Principles

For clarity, let the fluctuating electrical signal from the pressure transducer be m, the total signal be M, and the mean signal be M_0, then

$$M = M_0 + m \tag{B1}$$

The electronic problem is to modify the amplitude of m by the factor $M_0^{-2/3}$.

There are two basic approaches. These are (1) the dc component M_0 is separated from the ac component m and used to control the gain of an ac amplifier by the factor $M_0^{-2/3}$, and (2) the composite signal M is passed through an amplifier with a cube root characteristic. To explain the latter approach, note that if the output of the nonlinear characteristic is N $(= N_0 + n)$, and

$$N = KM^{1/3} \tag{B2}$$

where K is a constant, then

$$dN = \frac{K}{3} M_0^{-2/3}\, dM \tag{B3}$$

which is the same as the desired

$$n \sim M_0^{-2/3}\ m \tag{B4}$$

It is of value to note the magnitudes involved here. A 5:1 velocity ratio covers the range for most individual aircraft. This means a range of M of 25:1, typically 5 volts to 0.2 volts for standard 5 volt type pressure transducers. The range of ac gain variation needed is thus 8.55:1. This gain m involves frequencies in the 2-30 cps range.

Both of these approaches use the properties of silicon diodes. For completeness an addendum to this appendix (beginning on page B-25) reviews the pertinent characteristics of this device.

B. Mechanical Method

Before looking at electronic methods of accomplishing the $n \sim M_0^{-2/3}$ m relationship, it is interesting to investigate a possible mechanical method of doing the job. Conceptually at least, the sensor itself can be mechanically modified so the diaphragm stiffness varies with Δp. This stiffness function would be adjusted so the sensor output is $\sim(\Delta p)^{1/3}$, and thus, for a particular density since in this case $N = \Delta p \sim \rho U^2$, $n \sim U_0^{-4/3}$ u, which is the desired gain change in terms of u and U_0 comparable to Eq. (B4).

Previous work by MRI on obtaining a $(\Delta p)^{1/2}$ voltage function out of a diaphragm suggested that a $(\Delta p)^{1/3}$ might actually be obtainable even for the high frequencies to 30 cps required here. Actual tests on a low frequency type $(\Delta p)^{1/3}$ diaphragm helped support this contention.

The diaphragm is positioned over a series of concentric adjustable rings, so positioned that the diaphragm center displacement is approximately $(\Delta p)^{1/3}$. The diaphragm is sealed with a thin covering layer of rubber-like material. Slits in the diaphragm provide a trimming effect.

This approach was not pursued further in this project because it was felt that electronic methods utilizing a standard proven pressure transducer would be preferable. There is a basic problem with the nonlinear pressure transducer. Although the relationship of $N \sim (\Delta p)^{1/3}$ can be obtained with fair accuracy, the curve approximation is by straight line segments and so the $dN = n = 1/3\ (\Delta p_0)^{-2/3}\ d(\Delta p) \sim U_0^{-4/3}\ u$ relation is far less accurate. Stated more simply, it is the slope of the N vs Δp curve which is involved in the gain alteration, and the slope can change rather abruptly even though the N vs Δp curve is fairly accurate. Making the slope change smoothly is not impossible but appears far more awkward than electronic methods. The same slope-change principles are encountered in a subsequent section on electronic curve fitting.

C. Servo System Method

The gain of the ac signal before the filter, or the gain of the ac or average signal after the filter, can be varied as $M_0^{-2/3}$ by having the mean voltage M_0 control a servo-driven potentiometer which is wound for the correct

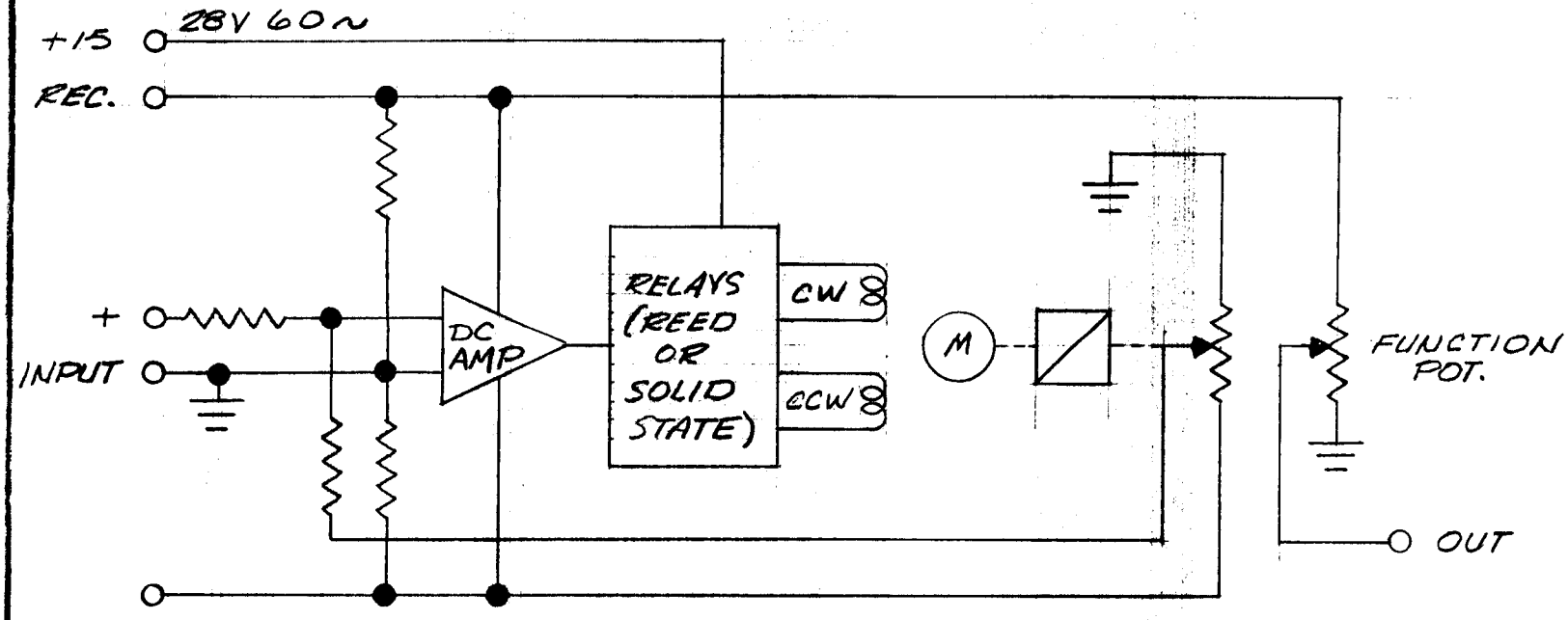

FIG B2. SIMPLIFIED SCHEMATIC, ON-OFF SERVO

function. The potentiometer would be a gain element. This is a straightforward solution. It is somewhat expensive and has the life and reliability problems of servo drives and potentiometers, and therefore is considered less desirable than electronic methods which will be discussed next. A simplified schematic of a suitable servo system is shown in Fig. B2.

D. Electronic Methods

1. The Gain-Controlled Amplifier

In this method the ac signal is separated from the mean signal M_o and put through a non-linear amplifier using a piece-wise linear approximation to the desired characteristic. Because the 2/3 function is not far from unity a simple "two line with initial bias" approximation was found adequate. The output of this amplifier drives an ac amplifier, the gain of which is controlled to be inversely proportional to M_{out}; thus, the output is proportional to $M_o^{-2/3}$.

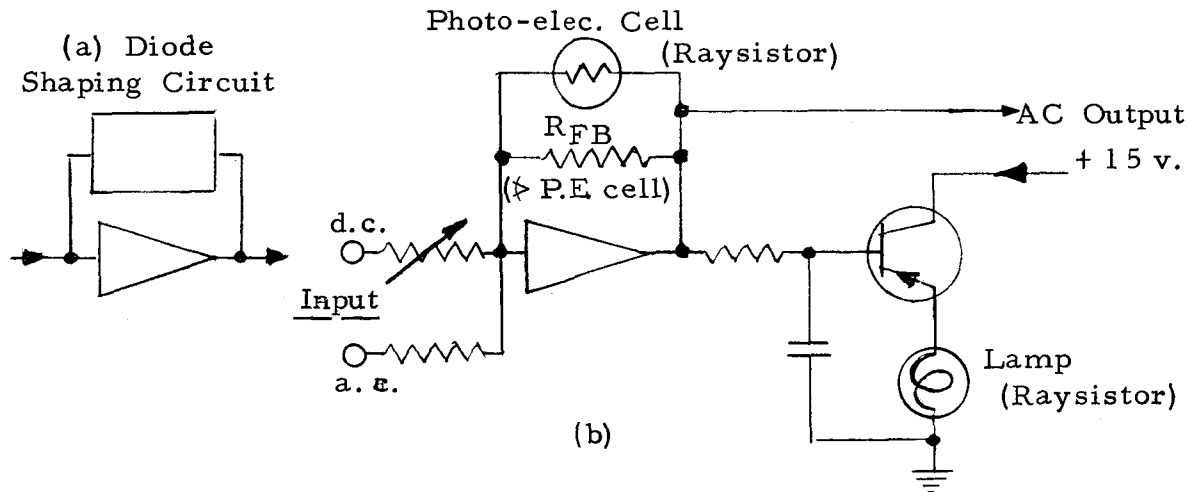

Fig. B3 Raysistor Circuit

A circuit schematic is shown in Fig. B3. A Raysistor is employed in the circuit for providing the gain control as a function of the reciprocal of a mean voltage. The transistor is functioning as an emitter follower to give sufficient current for the lamp. The reduced voltage at the lamp greatly enhances its operational life and decreases self-heating effects. Curves plotted with different Raysistor samples were encouragingly close. Advantages of this method are simplicity and low cost.

The system was breadboarded to check its overall operation. Problems were encountered with the relatively high current requirements of the Raysistor;

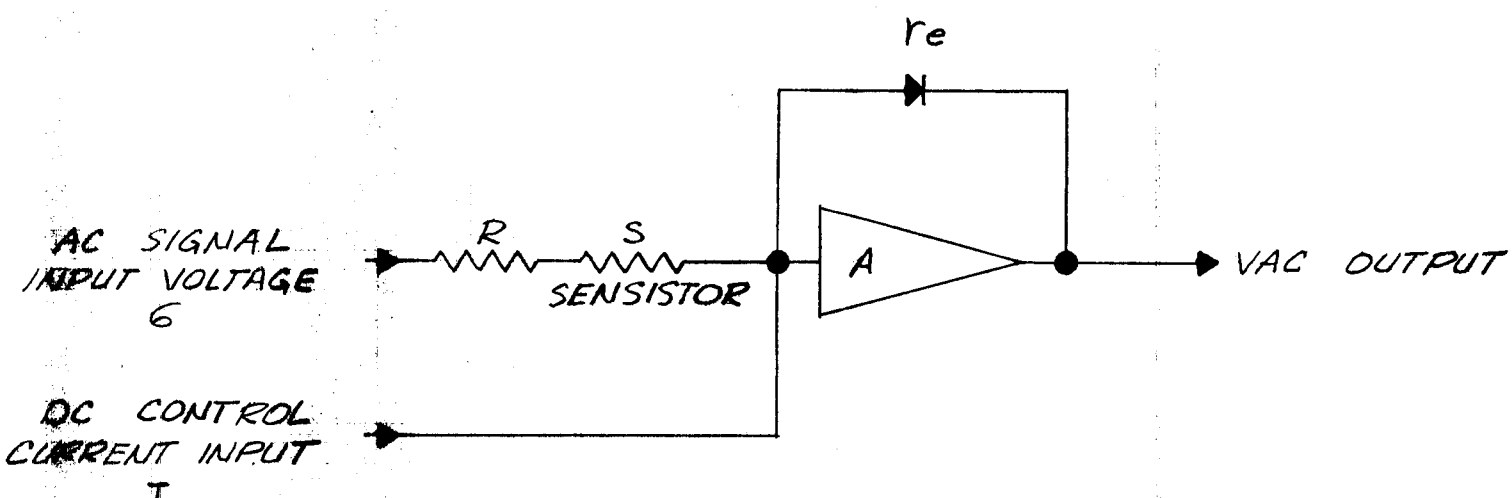

FIG. B4 GAIN CONTROLLED AMPLIFIER

and, from the short life and gain instabilities inherent in incandescent lamps and photoelectric cells (especially with respect to ambient and self-generated temperature effect). The solution was a modified design which is the (b) portion of Fig. B3. The (a) portion of the circuit was eliminated because the nonlinearity inherent in the Raysistor reciprocal circuit almost exactly added the necessary amount. The exact desired characteristic was obtained by reducing the lamp voltage with the series input resistor, and by increasing the amplifier feedback by R_{FB}.

As shown by equation (B22), page B-25, current dependence of the dynamic resistance of a silicon diode was used in the gain controlled amplifier configuration shown in Fig. B4. If the amplifier gain (A) is made infinitely large and if the output ac voltage (V_{AC}) is small compared to 1/c ($\sim$37 mV), then the output is related to the input (σ) by:

$$\frac{V_{AC}}{\sigma} = \frac{r_e}{R + S} = \frac{\alpha k T}{qI (R + S)} \qquad (B5)$$

Thus the gain of this amplifier is inversely proportional to the control current (I). The ratio of the resistance of the sensistor (S) to that of the stable resistance (R) is chosen to cancel the temperature dependence of r_e.

This technique has the advantage of being proportional to diode characteristics. For typical diodes at constant current the value of r_e may vary between diodes by as much as 20 per cent. Also, it may be difficult to match the sensistor value to each diode temperature characteristic without extensive temperature tests on each unit. These problems could be reduced by selecting diodes and by placing them in a temperature stabilized crystal oven.

Because the output ac voltage must be small compared to 1/c, further amplification by nearly 1000 will be necessary. Such a high gain may cause significant noise and pickup problems. The output signal level can be increased by placing as many as five diodes in series, reducing the gain required to the order of 200.

2. The Cube Root Amplifier

The basis of this method was given previously in Eqs. (B2), (B3), and (B4). The problem of accuracy was brought up in connection with the mechanical method. To summarize, a piece-wise linear approach cannot be used because the differentiation prodedure to recover the ac signal is too sensitive to the breakpoints in the amplifier gain curve.

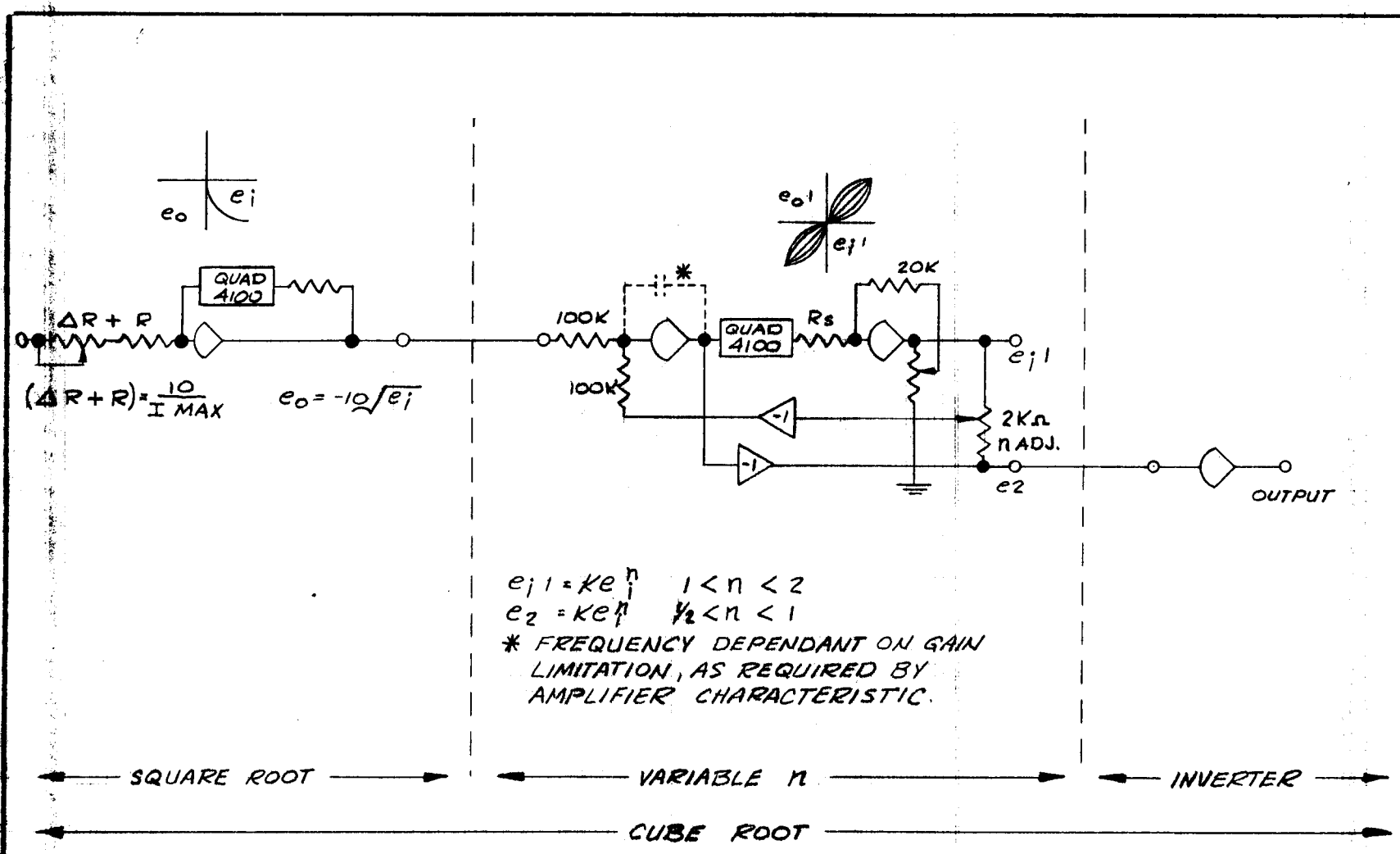

FIG B5 CUBE ROOT FUNCTION USING BOURNS QUADRATRON EXPONENTIAL RESISTORS

The application of the Bourns Model 4100 Quadratron Exponential Resistor to arrive at the cube root is as shown in Fig. B5.

The circuit operation is as follows. By applying the input signal to the square root circuit, the output $e^{1/2}$ is then fed into the input of the variable n function where n is adjusted to 2/3. The variable n function will then raise the $e^{1/2}$ signal to the 2/3 power, giving an output of $e^{1/3}$. An inverting amplifier at the output, designated e_2 on Fig. B4 in the variable n circuit, will be required in order to give the positive voltage solution.

As described, the device uses the non-linear electrical characteristics of silicon carbide. The desired within tolerance characteristic is adjusted by calibration of the individual device with a series resistor at a given room temperature, typically 25°C.

The circuit includes diodes which may cause temperature compensation problems and, without breadboarding the circuit and testing it over the temperature range, it is uncertain whether the required accuracy can be obtained. It should be noted that the manufacturer intends the device to be used as a laboratory instrument, at room ambient, and supplied with each device an R_s calibration for this purpose. The complete system is relatively complex, requiring six amplifiers and two Quadratrons.

The application of a silicon diode to achieve a cube root function is shown in Fig. B6. The first amplifier utilizing D1 and D2 has an output (V_3) proportional to the logarithm of the input voltage. This signal, after attenuation by a factor of three, enters an amplifier, consisting of D3 and D4, which has an exponential gain characteristic. The output is thus proportional to the cube root of the input.

For the following analysis the dc amplifiers are assumed to have infinite gain and no offset voltage. With this approximation the input current (i), given by V_s/R_1, must all flow in the feedback diode D1. The voltage V_2 is then given by:

$$V_2 = -\frac{1}{c_1} \ln\left(\frac{i}{i_1} - 1\right) \qquad \text{(B6)}$$

where:

c_1 = voltage constant of D1

i_1 = leakage current of D1

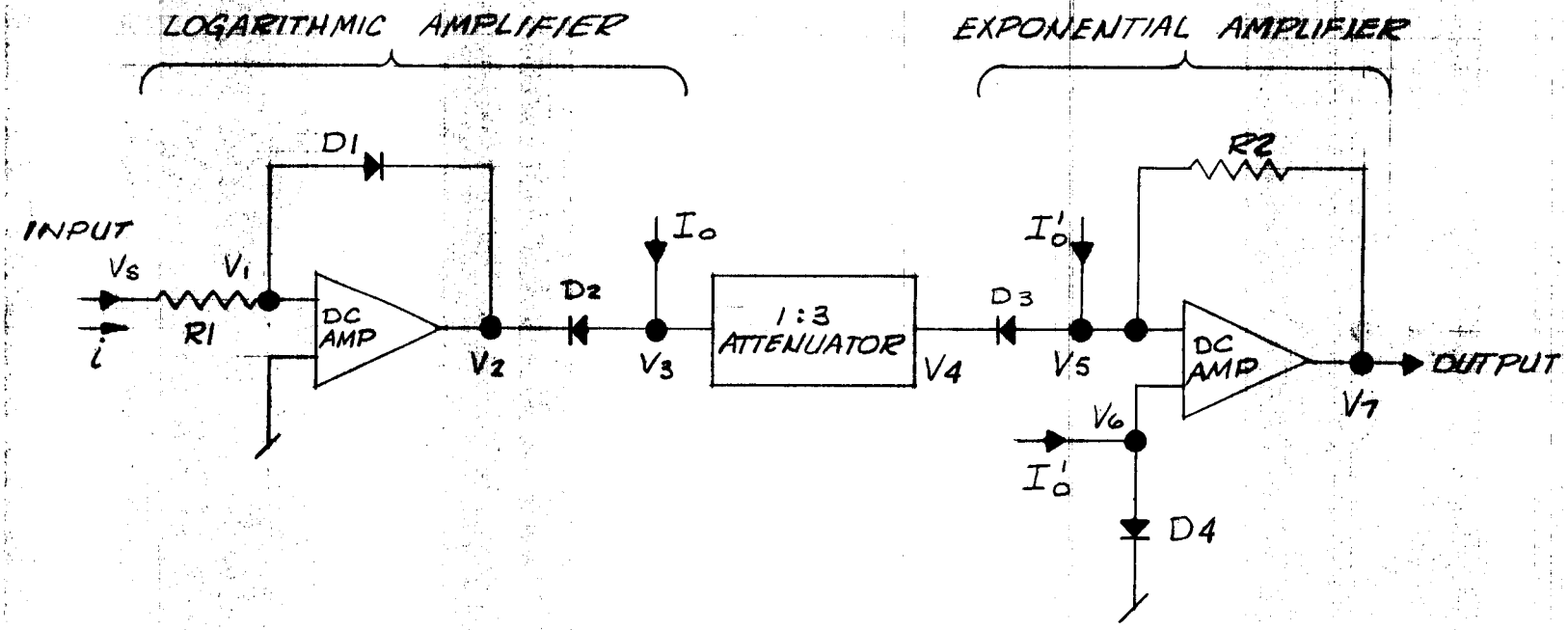

FIG 86 CUBE ROOT DIODE AMPLIFIER

Because D2 is biased at a fixed current I_o, the amplifier output voltage V_3 is given by:

$$V_3 = \frac{1}{C_2} \left\{ \ln\left(\frac{I_o}{i_2} - 1\right) - \frac{c_2}{c_1} \ln\left(\frac{i}{i_1} - 1\right) \right\} \qquad (B7)$$

For diodes matches such that $c_1 = c_2 = c$ and for $I_o \gg i_2$ and $i \gg i_1$, then:

$$V_3 \cong -\frac{1}{c} \ln\left\{ \left(\frac{i}{I_o}\right)\left(\frac{i_2}{i_1}\right) \right\} \qquad (B8)$$

producing the required logarithmic response.

For the exponential amplifier, the dc amplifier is referenced to V_6 by the forward current I_o' flowing in D4. For an ideal amplifier V_5 must equal V_6, and, if D3 is matched to D4, the bias current (I_o') at the summing junction (V_5) all flows in D3 when V_4 are related by:

$$V_7 = R_2 I_o' \left[\frac{i_3}{i_4}\right] e^{-cV_4} \qquad (B9)$$

where i_3 = leakage current of D3; i_4 = leakage current of D4; and,

if $c_3 = c_4 = c$ and if $I_o' \gg i_4$ and $(V_7 - V_5)/R_2 \gg i_3$.

Because $V_4 = 1/3\ V_3$, the total system gain is given by:

$$V_7 = \sqrt[3]{V_s} \left[\frac{R_2 I_o'}{\sqrt[3]{R_1 I_o}}\right] \times \left[\frac{i_3}{i_4} \sqrt[3]{\frac{i_2}{i_1}}\right] \qquad (B10)$$

If the diodes are selected to have equal leakage currents, then the second bracket in equation B10 becomes one, and the gain depends only on fixed resistors and currents.

The advantage to this system is that it does not depend on linear approximations to a gain curve and, with sufficient matching of diodes, is independent of diode characteristics. Even though diodes with matched forward characteristics and leakage currents are commercially available (e.g., Fairchild FD3389), the stringent matching requirements may cause production difficulties. Furthermore the signals must still be small compared to $1/c$ ($\sim$37 m V) unless several diodes in series are employed. The need for further amplification remains in either case.

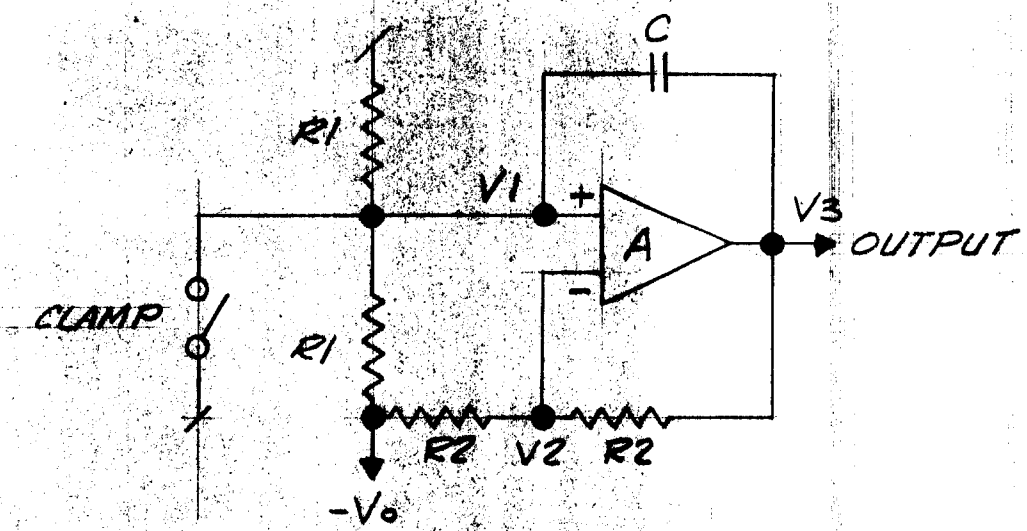

FIG B7 POSITIVE FEEDBACK AMPLIFIER

Even with matched diodes the exponential dependence of leakage current on temperature causes further difficulties. For a typical diode, the leakage current as a function of temperature (T) is given by:

$$i_L = (1.3 \times 10^{-10}\ A)\ \exp(T/15°C) \qquad (B11)$$

For this case the leakage current has a temperature coefficient of 6.7%/°C. By matching diodes as in the logarithmic amplifier, ref. 5 reduced this coefficient to 1.8%/°C. Because the gain is proportional to the ratio of leakage currents, 5 percent accuracy will be achieved only if the temperature is constant within 2.8°C. This requirement makes a temperature stabilized oven mandatory for the diodes D1 to D4. This temperature accuracy would not be difficult for most commercially available crystal ovens.

3. Positive Feedback Amplifiers

The strong dependence on device characteristics and on temperature of the various diode amplifiers indicates the advisability of alternate approaches. One such approach employs the exponential characteristic of positive feedback amplifiers.

A typical amplifier configuration is shown in Figure B7. The amplifier A is a differential dc amplifier with positive feedback via c and negative feedback via R_2. For the following analysis A will be assumed infinitely large, and no dc amplifier voltage offsets will be considered. In this approximation V_1 and V_2 must be equal. Several commercially available integrated circuit amplifiers would be suitable for this application.

When the clamp switch (probably a saturated transistor) is closed, the positive feedback path is shorted out, and the output (V_3) rests stably at a voltage V_0. Because the capacitor has an initial charge of CV_0, the output will rise exponentially with time as soon as the clamp switch is opened. For the component values shown in Fig. B7 the output voltage (V_3) is given by:

$$V_3 = V_0\ \exp(2t/R_1C) \qquad (B12)$$

where t = time after the clamp switch was opened.

For the infinite gain approximation, all quantities in equation (B12) are determined by stable voltages, resistors and capacitors, and no critical dependence on semiconductor parameters is present.

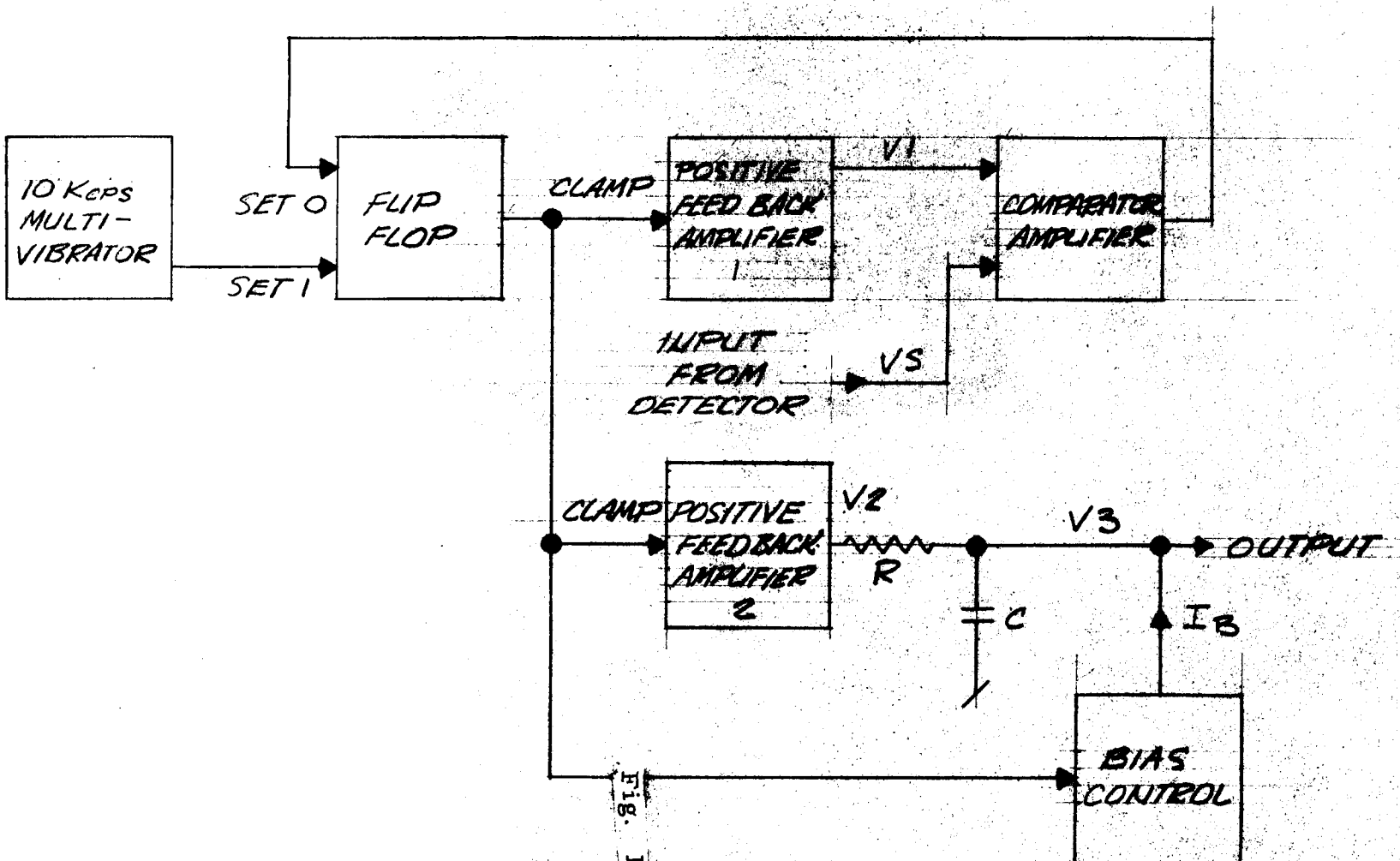

FIG.B8 CUBE ROOT SYSTEM USING AVERAGING

One method for utilizing the exponential characteristic of a positive feedback amplifier to construct a cube root amplifier is illustrated in Fig. B8. The system is synchronized to a stable 10 Kcps clock multivibrator. The flip-flop is normally in the "zero" state, causing both positive feedback amplifiers to be clamped. On the leading edge of a clock pulse (see Fig. B9) the flip-flop is set to the "one" state, releasing the clamp on both positive feedback amplifiers. When the output voltage of amplifier No. 1 reaches the level of the input voltage (V_s), the comparator amplifier triggers the flip-flop back to the "zero" state, resetting both positive feedback amplifiers. The output of the second amplifier is averaged by an RC circuit, and an appropriate bias current is subtracted.

Assume that the response of the first amplifier is given by:

$$V_1 = V_{o1} \exp(t/\tau_1) \tag{B13}$$

Then the time (t_1) for the output (V_1) to reach the input voltage (V_s) is:

$$t_1 = \tau_1 \ln (V_s/V_{o1}) \tag{B14}$$

The output of the second amplifier is then given by:

$$\begin{aligned} V_2 &= V_{o2} \exp(t/\tau_2) \quad 0 < t < t_1 \\ V_2 &= V_{o2} \qquad\qquad\quad t_1 < t < T \end{aligned} \tag{B15}$$

The average value of V_2 found by integrating equation (B15) is then:

$$\overline{V}_2 = \frac{\tau_2 V_{o2}}{T}\left(\frac{V_s}{V_{o1}}\right)^{\tau_1/\tau_2} - V_{o2}\left[\frac{\tau_2 - t_1}{T} - 1\right] \tag{B16}$$

If τ_2 is chosen equal to 3 τ_1 and if the term proportional to t_1 is cancelled, the average of V_2 is proportional to $\sqrt[3]{V_s}$. The cancellation of the t_1 term is provided by controlling the bias current with the flip-flop output so that:

$$\begin{aligned} I_B &= \frac{V_{o2}\,\tau_2}{RT} \qquad 0 < t < t_1 \\ I_B &= \frac{V_{o2}}{R}\left[\frac{\tau_2}{T} - 1\right] \quad t_1 < t < T \end{aligned} \tag{B17}$$

If $RC \gg T$ and if the changes in V_s are small during an RC period, then:

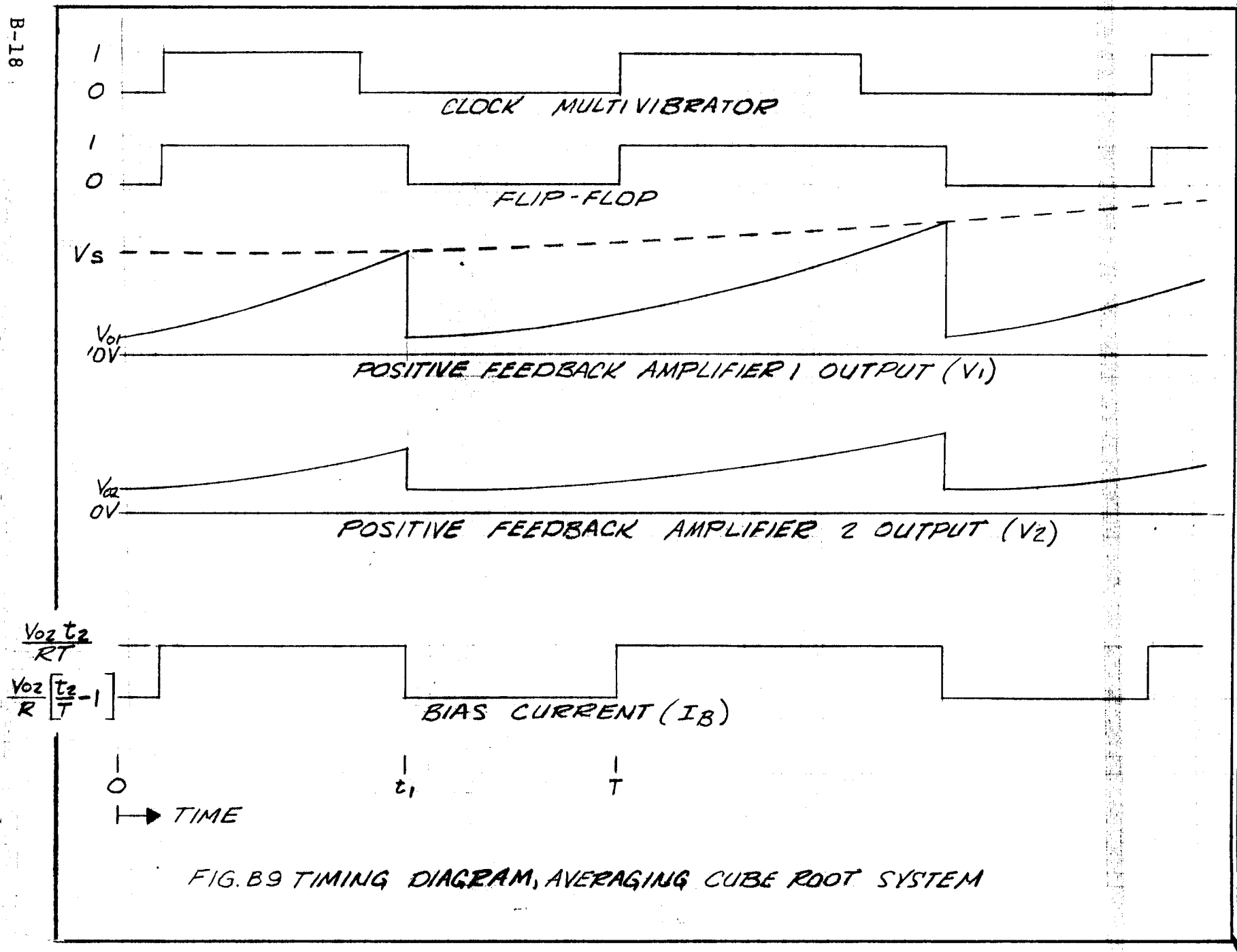

FIG. B9 TIMING DIAGRAM, AVERAGING CUBE ROOT SYSTEM

$$V_3 = \frac{\tau_2 V_{02}}{T \sqrt[3]{V_{01}}} \sqrt[3]{V_s} \qquad \text{(B18)}$$

(The RC filter shown in Fig. B8 can actually be part of the band-pass filter.)

This scheme has the advantage of not depending critically on semiconductor properties and should not be strongly temperature dependent. No oven should be necessary if the dc amplifiers are properly constructed. Furthermore, the output dc signals will be several volts, eliminating the need for subsequent large gain ac amplifiers. Preliminary estimates indicate that a 25:1 dynamic range is feasible with 5 percent of full scale accuracy. The general complexity of this scheme appears comparable to the other techniques, and no ultra-stable power supplies, matching procedures or sensitive adjustments are required.

4. Cube Root System Using Peak Detection

From Eqs. (B17) and (B18) it can be seen that with the averaging technique a stable multivibrator, which generates the period T, and a stable switched bias current are necessary. If, however, the peak of the output signal from the second positive feedback amplifier were detected, then the above problems disappear. Such a system is illustrated in Fig. B10, with the timing sequence shown in Fig. B11.

In this approach, an output pulse from a single-shot clamps the positive feedback amplifiers as did the flip-flop output in the previous technique. When the single-shot times out in a time T, both amplifiers are unclamped simultaneously, and their outputs rise exponentially. When the output voltage (V_1) of the first amplifier equals the input voltage (V_s), the single-shot is again triggered via the comparator amplifier, resetting the positive feedback amplifiers. At this time (t_1) the sample and hold circuit is programmed to make the output voltage (V_3) equal to the peak voltage of the second positive feedback amplifier. Thus:

$$V_3 = V_{02} \left(\frac{V_s}{V_{01}} \right)^{\tau_1 / \tau_2} \qquad \text{(B19)}$$

If $\tau_2 = \beta \tau_1$, then the desired cube root dependence is achieved.

This technique replaces the problem of producing a stable multivibrator and switchable current bias with the problem of designing an accurate sample and hold system.

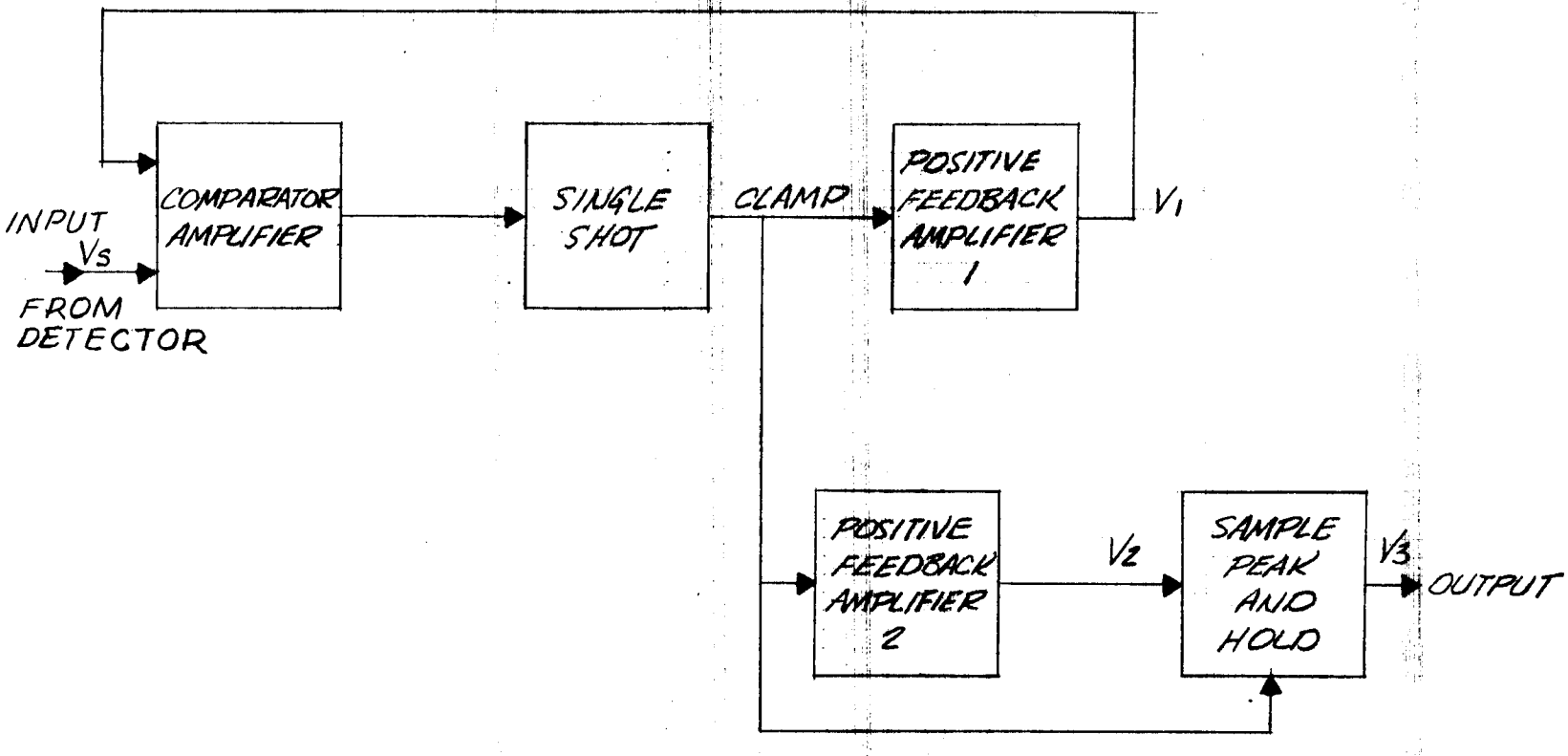

FIG B10 CUBE ROOT SYSTEM USING PEAK DETECTION

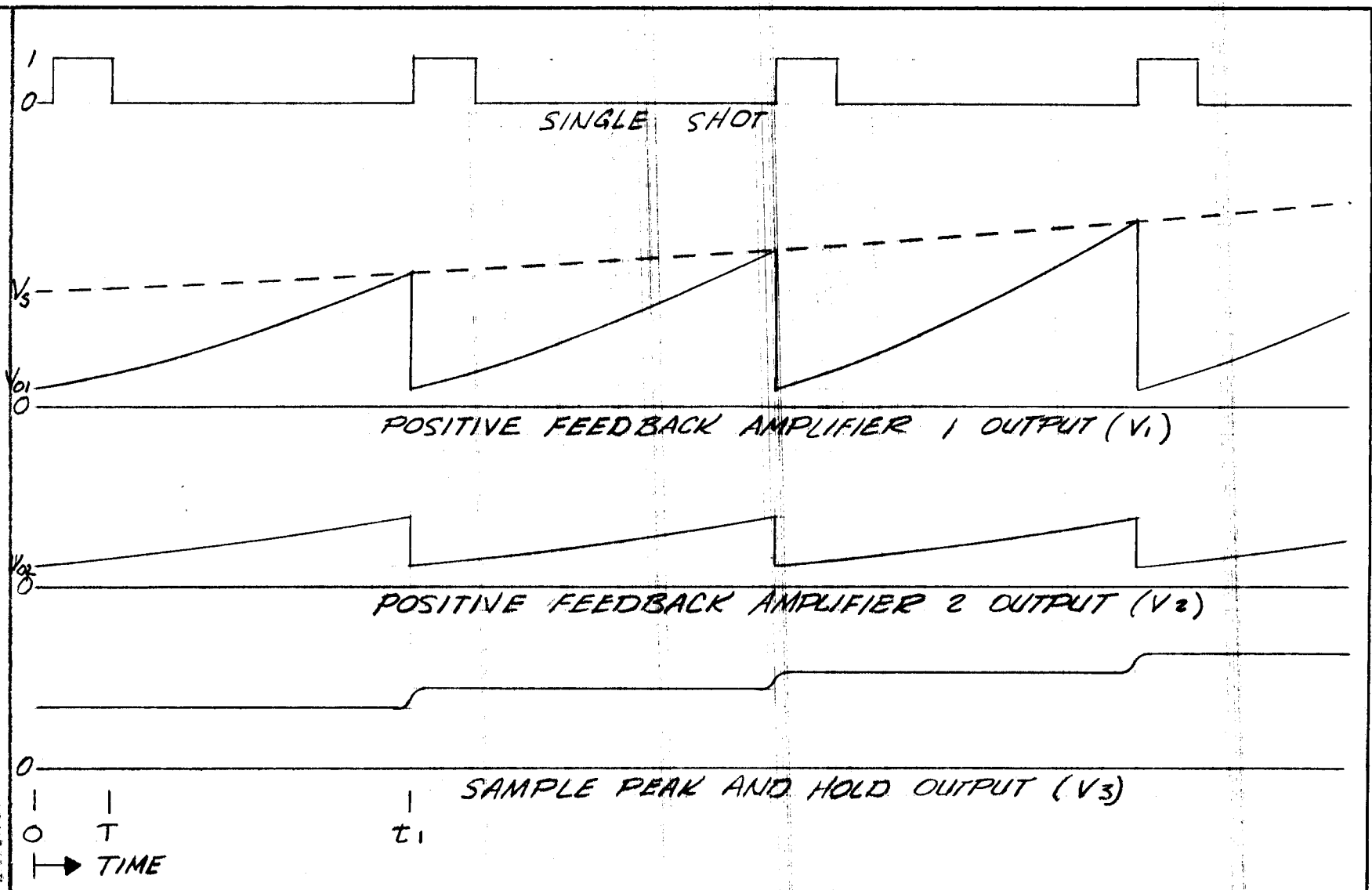

FIG. B11 TIMING DIAGRAM, PEAK DETECTION CUBE ROOT SYSTEM

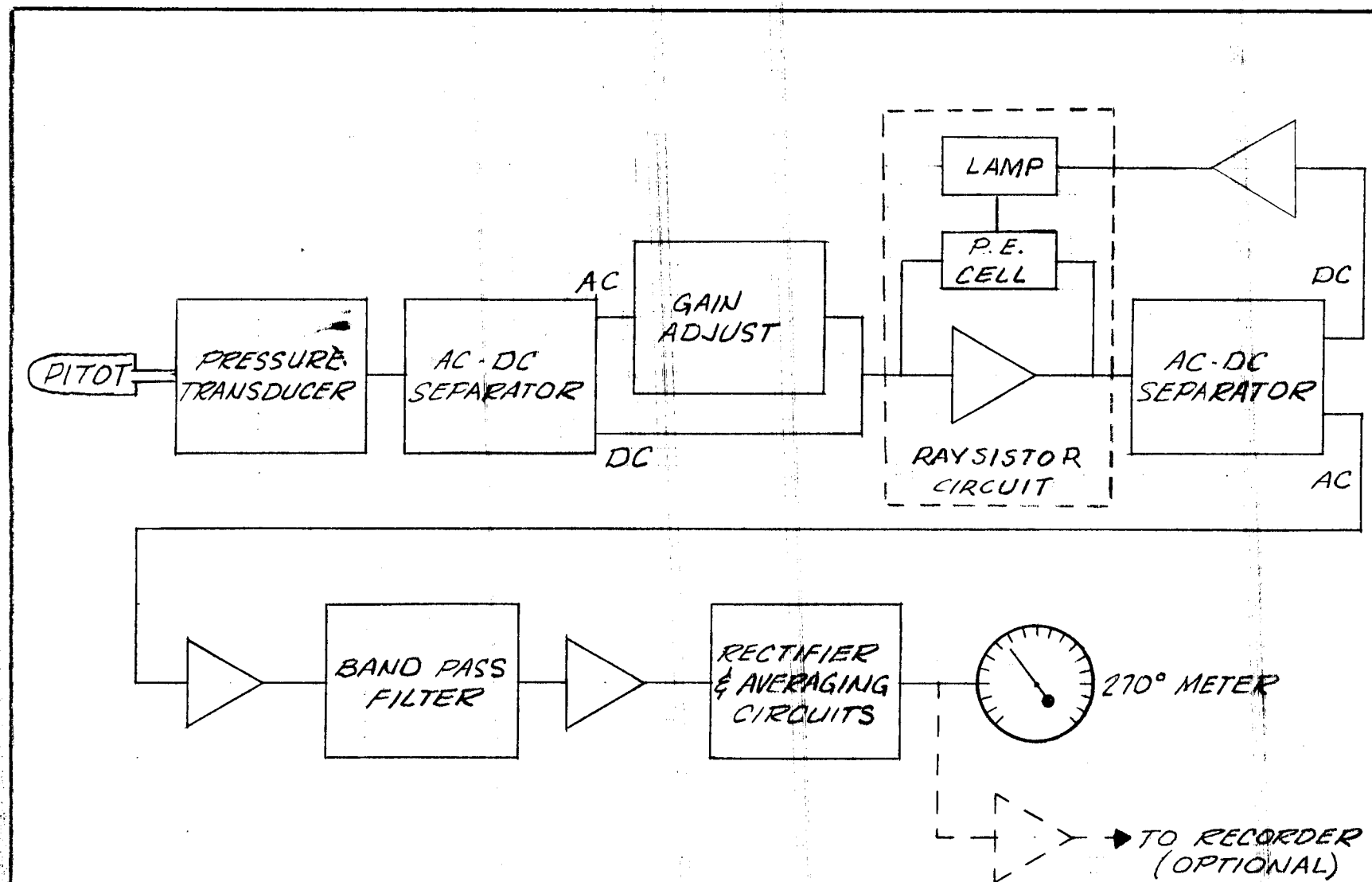

FIG. B-12 UITS SIMPLIFIED BLOCK DIAGRAM

5. Optimum Design

Figure B12 is a block diagram of the recommended design. The gain control is obtained by the method shown in Fig. B3.

Calibration of the system is provided by an a-c signal source superimposed on a d-c bias which is set at two points on the curve to obtain 50 per cent and 100 per cent levels. For check-out procedure this operation could be programmed by a simple pushbutton switch.

E. Alternative Accelerometer System

R can be measured by using a vertical accelerometer instead of a differential pressure pickup to provide the fluctuating voltage to the system electronics; a mean voltage from the differential pickup is still required for the system gain control. This technique may prove useful in special cases. Since σ_h, the RMS value of accelerations causing the human feel of turbulence, was assumed to represent a particular frequency or band of frequencies in the 1 to 5 cps band, σ_h can be found by an accelerometer. By inverting Eq. (8),

$$R \sim \sigma_h \, (IAS)^{-4/3} \tag{B20}$$

where σ_h is now the RMS voltage from the accelerometer coming through a band-pass filter within the 1 to 5 cps band. Equation (B20) shows there must still be an a-c gain variation with mean indicated airspeed of $(IAS)^{-4/3}$ or $(\Delta p)^{-2/3}$. Thus the final UITS circuitry shown on Fig. B12 will work with a vertical accelerometer output substituting for the pressure transducer a-c output.

This technique offers the virtues of (a) utilizing a transducer which does not have to be located close to a pitot tube, (b) measuring the same turbulent component which causes primary gust loads (thus eliminating the need for turbulent isotropy in the concept), and (c) measuring the variable which should relate well to the human feel of turbulence; it has the negative features that (a) it requires two transducers (an accelerometer for the fluctuating signal and the Δp transducer for gain variations), (b) the constant of proportionality in Eq. (B20) is different for each airplane and even varies strongly for a single airplane having large gross weight variations, and (c) the instrument must use a narrower filter frequency band than is used with the complete pressure system (because the pass band must lie above the frequency at which the lift response to turbulence is appreciably attenuated).

The principle behind the system can be understood by observing that the voltage fluctuation from the accelerometer transducer is U_0 × vertical turbulence, while the voltage fluctuation from the differential pressure transducer is U_1 × longitudinal turbulence. Since they have a similar U_0 dependence, either can be used for the fluctuating part of the circuit in Fig. B12.

The accelerometer should be located in the fuselage well ahead of the center of lift at the point where elevator controls do not introduce accelerations. Then elevator motions are not involved, and the indicated RMS accelerations will be proportional to the RMS accelerations at the CG for an aircraft with fixed controls.

Addendum: Properties of Silicon Diodes for Amplifier Applications

A brief resumé of pertinent properties of silicon diodes is presented.

Diode current (i) is related to the forward voltage (V) across the diode by the well known formula:

$$i = i_L(e^{cV} - 1)$$

where: i_L = diode leakage current, and c = constant. The constant is approximately given by:

$$c = \frac{q}{\alpha kT}$$

where: q = electron charge; k = Boltzman's constant; T = absolute temperature; α = constant of the order of 1.5

At 25C for typical diodes such as FD 306 and 1N916 and for forward currents between 1 μ A and 1 mA,

$$c \sim 1/37 \text{ m V}$$

$$i_L \sim 2 \times 10^{-11} \text{ A}$$

Both c and i_L are dependent on temperature. The constant α is nearly independent of temperature, resulting in c being inversely proportional to the absolute temperature. The leakage current is an an exponential function of temperature and doubles for about every 10C rise in temperature.

The forward dynamic resistance (r_e) of a diode with a dc bias current (i) is given by:

$$r_e = \frac{dV}{di} = \frac{1}{c(i + i_L)} = \frac{\alpha kT}{q(i + i_L)} \qquad \text{(B21)}$$

For $i \gg i_L$, this formula reduces to

$$r_e \sim \frac{\alpha kT}{qi} \qquad \text{(B22)}$$

Because r_e is proportional to the absolute temperature, it possesses a temperature coefficient of approximately 0.3 to 0.4%/°C. However, for signals small compared to $1/c$ ($\sim$37 m V), the dynamic resistance of a silicon diode is inversely proportional to bias current over three decades.

APPENDIX C

RELATIONSHIPS BETWEEN INSTRUMENT READING, AIRCRAFT RESPONSE, AND HUMAN FACTORS

A. Derivations for a Pressure-Type Sensor

In the inertial subrange of atmospheric turbulence, which includes the range of eddy sizes which are of greatest importance for gust loads on ordinary aircraft, the turbulence has simple statistical properties. It is isotropic, and the turbulent spectra can be closely approximated by (see reference 1):

$$E(k) = \frac{3}{4}G(k) = C_2\, \epsilon^{2/3}\, k^{-5/3} \tag{C1}$$

Thus $\epsilon^{2/3}$ (or ϵ or $\epsilon^{1/3}$) is seen to be a measure of the turbulence intensity. Equivalently, in terms of frequency rather than wave number,

$$E(f) = \frac{3}{4}\, G(f) = C_2\, U_0^{2/3}\, \epsilon^{2/3}\, f^{-5/3} \tag{C2}$$

The aim of a measurement scheme is to ascertain ϵ in a simple manner. In the derivation in the original reference it was assumed that the sensor provides a voltage fluctuation, say m, corresponding to a small longitudinal turbulent fluctuation u, such that

$$m = U_0^{\,n}\, u \tag{C3}$$

With this sort of sensor it then turns out that the indicator will show ϵ, no matter what the speed or type of aircraft, if the amplitude of the fluctuating signal is altered by the factor $U_0^{-n-1/3}$. The main points of the derivation are as follows. With u having the spectrum $E(f)$ given by Eq. (C2), then m has the spectrum

$$J = C_2\, U_0^{2n+2/3}\, \epsilon^{2/3}\, f^{-5/3} \tag{C4}$$

If the fluctuating voltage m is put into a filter, if p represents the voltage out of the filter, and if the filter has a frequency response function $B(f)$ which is non-zero only for frequencies (wavelengths) pertaining to the inertial subrange, then

$$\overline{p^2} = \int_0^\infty J(f)B^2(f)\,df = C_2^{\,2}\, \epsilon^{2/3}\, U_0^{\,2n+2/3} \left[\int_0^\infty B^2(f)\, f^{-5/3}\, df\right] \tag{C5}$$

The term within brackets is a constant. The RMS value of a fluctuating voltage can be obtained electronically (the simplest method for fluctuations with a Gaussian distribution is to take the average of the rectified signal, times a suitable constant); so, with $r \equiv$ indicator output,

$$r = \sqrt{\overline{p^2}} = K_2 \, U_0^{\,n+1/3} \, \epsilon^{1/3} \tag{C6}$$

where all constants are lumped into K_2 .

The derivation given above applies to sensors with outputs fitting Eq. (C3) For example, when the sensor output is a voltage M directly proportional to velocity U (where U is the total velocity $U_0 + u$), then $M \sim U$, and so

$$\frac{dM}{dt} \sim \frac{dU}{dt} \; ; \; m \sim u \tag{C7}$$

meaning $n = 0$ in Eq. (C3). If $M \sim U^2$, as is typically the case with a pressure pickup measuring the dynamic pressure (assuming incompressibilty)

$$\frac{dM}{dt} \sim 2 \, U_0 \frac{dU}{dt} \; ; \; m \sim 2 \, U_0 \, u \tag{C8}$$

meaning $n = 1$ in Eq. (C3). A vane sensor would give $n = -1$ in Eq. (C3).

If the sensor is a pressure type and is used at various altitudes, then the density effects must be considered. In this case, instead of $M \sim U^2$ we have $M \sim \rho \, U^2$. Then

$$m \sim \rho \, U_0 \, u \tag{C9}$$

which is like Eq. (C3) for $n = 1$ except for the additional density factor. For the derivation of the Universal Turbulence System we must use Eq. (C9) instead of Eq. (C3). Then instead of Eq. (C4) we have

$$J(f) = C_2 \, \rho^2 \, U_0^{\,8/3} \, \epsilon^{2/3} \, f^{-5/3} \tag{C10}$$

Following the reasoning of Eqs. (C5) and (C6), and letting R denote the indicator output for this pressure-based system, we find

$$R \sim \rho \, U_0^{\,4/3} \, \epsilon^{1/3} \tag{C11}$$

Substituting M_o for ρU_o^2 then gives

$$R \sim M_o^{2/3} \left(\frac{\rho}{\rho_o}\right)^{1/3} \epsilon^{1/3} \qquad (C\ 12)$$

Thus if the magnitude of the fluctuating voltage is altered by a gain factor $M_o^{-2/3}$, then

$$R = K_3 \left(\frac{\rho}{\rho_o} \times \epsilon\right)^{1/3} \qquad (C\ 13)$$

We define this system to be the Universal Indicated Turbulence System (UITS). The indicator shows turbulence as $(\rho\epsilon/\rho_o)^{1/3}$ rather than just as $\epsilon^{1/3}$, but the indication is still universal inasmuch as the same turbulent intensity level would be shown on this indicator on any airplane flying at any air speed. When actually applying the measurement to aircraft response there will be additional considerations relating to density, so in the practical sense the $(\rho\epsilon/\rho_o)^{1/3}$ quantity is just as simple to use as $\epsilon^{1/3}$ would be. In fact, as will be shown later, the $(\rho\epsilon/\rho_o)^{1/3}$ is actually a better quantity than $\epsilon^{1/3}$ to use for aircraft load calculations.

B. Relationship Between R and RMS Aircraft Accelerations

The UITS concept involves a linear relationship between the instrument reading, R, where $R = (\rho\epsilon/\rho_o)^{1/3}$, and the RMS value of aircraft vertical accelerations, σ_g. The constant of proportionality may depend on aircraft characteristics, air speed, and density. The relationship is based on the assumption that the vertical power spectral density, G(k), is a unique function of ϵ from Eq. (C 1):

$$G(k) = \frac{4}{3} C_2\ \epsilon^{2/3}\ k^{-5/3} \qquad (C\ 14)$$

For wavelengths beyond the interial subrange, other spectra should apply, spectra which can still be assumed to be related to ϵ for the ranges and accuracies required for ordinary gust load calculations. The complete derivation of σ_g versus R for the general case is given later. It is instructive here to show the form of the solution for the case where the gust loads are all from turbulent wavelengths covered by Eq. (C 14).

For this derivation, we get a feeling for the physical picture by noting how a rigid, non-pitching aircraft responds to an abrupt vertical velocity change w_o

at $t = 0$. Solving the simple response equation then gives the vertical acceleration as

$$\ddot{z} = B \rho U_o w_o e^{-B \rho U_o t} \tag{C15}$$

where B is a constant depending on aircraft characteristics (wing loading and slope of the lift curve), ρ is air density, and U_o is air speed. Thus the acceleration magnitude is proportional to ρU_o and the intensity of the vertical turbulence, while the shape of the aircraft motion history is a function of $\rho U_o t$ which is $\rho \times$ distance. Therefore one sees that for continuous turbulence the response function relating acceleration to turbulent vertical velocity will have a unique shape when plotted versus $(\rho\lambda)^{-1}$ or k/ρ and will have an amplitude proportional to ρU_o.

Transforming Eq. (C14) to the same variable gives

$$G(\frac{k}{\rho}) = \frac{4}{3} C_2 \epsilon^{2/3} \rho^{-2/3} (\frac{k}{\rho})^{-5/3} \tag{C16}$$

Thus there is a spectrum, Eq. (C16) and a response characteristic with amplitude varying only as ρU_o when plotted as a function of k/ρ, from which it follows that

$$\sigma_g^2 \sim \rho^2 U_o^2 \int_0^\infty \left[\text{resp. char.} (\frac{k}{\rho})\right]^2 G(\frac{k}{\rho}) \, d(\frac{k}{\rho}) \tag{C17}$$

The shapes of the response characteristic and the turbulent spectrum are such that, using Eq. (C14) and performing the integration gives

$$\sigma_g^2 \sim \epsilon^{2/3} \rho^{4/3} U_o^2 \tag{C18}$$

and thus, since $\rho_o (IAS)^2 = \rho U_o^2$,

$$\sigma_g \sim \rho^{-1/6} (IAS) (\frac{\rho}{\rho_o} \times \epsilon)^{1/3} \tag{C19}$$

$$\sigma_g \sim \rho^{-1/6} (IAS) R \tag{C20}$$

The constant of proportionality relating σ_g and R in Eq. (C20) depends only on the aircraft wing loading and geometry. The variation of $\rho^{-1/6}$ with altitude is very small, from sea level to 40,000 feet being always within 10 per cent of the value at 20,000 feet; thus for the general accuracy required of the UITS one often can use the simple relation

$$\sigma_g \sim IAS \times R \tag{C21}$$

C. Derivation of σ_g Versus R Relationships

In the inertial subrange of eddy sizes, the spectral density of vertical velocity is given by Eq. (C14). For larger eddies, smaller values of the wave number k, the spectrum tends to flatten out. For the purposes of this analysis this effect will be approximated by assuming that the turbulence spectrum is given by Eq. (C14) for wave numbers greater than some constant k_1 and the spectrum is constant for wave numbers less than k_1.

For subsequent calculations it is desirable to have the turbulence spectrum in terms of frequency, ω, rather than wave number, thus

$$\omega = 2\pi k U_o \tag{C22}$$

where U_o is the average (or steady state) aircraft speed. The spectrum conversion from wave number to frequency is

$$G(\omega) = \frac{1}{2\pi U_o} G(k) \tag{C23}$$

or

$$G(\omega) = \begin{cases} \frac{2^{8/3}}{3} \pi^{2/3} C_2 \epsilon^{2/3} U_o{}^{2/3} \omega_1{}^{-5/3}, & 0 \le \omega \le \omega_1 \\ \frac{2^{8/3}}{3} \pi^{2/3} C_2 \epsilon^{2/3} U_o{}^{2/3} \omega^{-5/3}, & \omega_1 \le \omega \end{cases} \tag{C24}$$

where $\omega_1 = 2\pi k_1 U_o$

1. Aircraft Transfer Function

As the aircraft pitching motions will be at least partially constrained by the pilot or autopilot, we will assume that the aircraft's only degree-of-freedom is vertical translation. We will also neglect unsteady aerodynamic effects because they only become important at very high frequencies where there is little turbulence input. Under these assumptions the aircraft acceleration response ($\ddot{z}$) to a vertical gust (w_g) is given by the transfer function

$$\frac{\ddot{z}}{w_g} = \frac{ps}{s+p} \tag{C25}$$

where s = Laplace operator, and

$$p = \frac{\rho g S U_o C_{L_\alpha}}{2 W} \tag{C26}$$

ρ = atmospheric density

g = acceleration due to gravity

S = aircraft wing area

C_{L_α} = slope of aircraft lift coefficient (per radian) with lift coefficient reference area equal to S

W = aircraft weight

2. RMS Acceleration

The mean square acceleration of the aircraft is obtained by integrating the aircraft acceleration power spectrum, which equals the turbulence spectrum multiplied by the magnitude squared of the $\ddot{z}/w_g$ transfer function, i.e.,

$$\sigma_{\ddot{z}}^2 = \int_o^\infty \frac{p^2 \omega^2}{\omega^2 + p^2} G(\omega)\, d\omega \tag{C27}$$

Using Eq. (C24) in Eq. (C27) we have

$$\sigma_{\ddot{z}}^2 = \frac{2^{8/3}}{3} \pi^{2/3} C_2 \epsilon^{2/3} U_o^{2/3} p^2 \left[\omega_1^{-5/3} \int_o^{\omega_1} \frac{\omega^2}{\omega^2 + p^2} d\omega + \int_{\omega_1}^\infty \frac{\omega^{1/3}}{\omega^2 + p^2} d\omega \right] \tag{C28}$$

The first integral in Eq. (C28) is quite simple and can be found in most tables of integrals.

$$\int_o^{\omega_1} \frac{\omega^2\, d\omega}{\omega^2 + p^2} = \left[\omega - p \tan^{-1} \frac{\omega}{p} \right]_o^{\omega_1} = \omega_1 - p \tan^{-1} \frac{\omega_1}{p} \tag{C29}$$

The second integral is more complicated and we have to use a change of variable to solve it. If we let

$$y = \omega^{2/3} \tag{C30}$$

then

$$\int \frac{\omega^{1/3}\, d\omega}{\omega^2 + p^2} = \frac{3}{2} \int \frac{y\, dy}{y^3 + p^2}$$

$$= \frac{p^{-2/3}}{2} \int \left[\frac{y + p^{2/3}}{y^2 - y p^{2/3} + p^{4/3}} - \frac{1}{y + p^{2/3}} \right] dy \qquad (C31)$$

Now both integrals on the right side of Eq. (C31) can be found in most integral tables.

$$\int \frac{\omega^{1/3} d\omega}{\omega^2 + p^2} = \frac{p^{-2/3}}{2} \left[\frac{1}{2} \log_e (y^2 - y p^{2/3} + p^{4/3}) \right.$$

$$\left. + \sqrt{3} \tan^{-1} \left(\frac{2y - p^{2/3}}{\sqrt{3}\, p^{2/3}} \right) - \log_e (y + p^{2/3}) \right]$$

$$= \frac{p^{-2/3}}{4} \left[\log_e \frac{(y^2 - y p^{2/3} + p^{4/3})}{(y + p^{2/3})^2} + 2\sqrt{3} \tan^{-1} \left(\frac{2y - p^{2/3}}{\sqrt{3}\, p^{2/3}} \right) \right] \qquad (C32)$$

At this point it becomes convenient to introduce the nondimensional parameter, X_1, defined by

$$X_1 = \frac{\omega_1}{p} \qquad (C33)$$

Then

$$y = (p X_1)^{2/3} \qquad (C34)$$

Substituting Eq. (C34) and evaluating the integral between limits ω_1 to ∞

$$\int_{\omega_1}^{\infty} \frac{\omega^{1/3} d\omega}{\omega^2 + p^2} = \frac{p^{-2/3}}{4} \left[- \log_e \frac{(X_1^{4/3} - X_1^{2/3} + 1)}{(X_1^{2/3} + 1)^2} \right.$$

$$\left. + \sqrt{3}\pi - 2\sqrt{3} \tan^{-1} \left(\frac{2 X_1^{2/3} - 1}{\sqrt{3}} \right) \right] \qquad (C35)$$

By substitution of Eqs. (C24) and (C26)

$$X_1 = \frac{\omega_1}{p} = \frac{4\pi k_1 W}{\rho g S C_{L_\alpha}} \qquad (C36)$$

Combining Eqs. (C28), (C29), (C30), and (C36) we get

$$\sigma_{\ddot{z}}^2 = \frac{2^{8/3}}{3} \pi^{2/3} C_2\, \epsilon^{2/3} U_o^{2/3} p^{4/3} f(X_1) \qquad (C37)$$

where

$$f(X_1) = X_1^{-2/3} - X_1^{-6/3} \tan^{-1} X_1 + \frac{\sqrt{3}\,\pi}{4}$$

$$- \frac{\sqrt{3}}{2} \tan^{-1}\left(\frac{2 X_1^{2/3} - 1}{\sqrt{3}}\right) - \frac{1}{4} \log_e \frac{(X_1^{4/3} - X_1^{2/3} + 1)}{(X_1^{2/3} + 1)^2} \qquad (C\,38)$$

Let us now make several substitutions. First, it is common to refer to accelerations in g's so introducing

$$\sigma_g = \frac{\sigma \ddot{z}}{g} \qquad (C\,39)$$

We also want to relate the magnitude of the turbulence to the reading of the Universal Turbulence Meter, R .

$$R = \left[\frac{\rho \epsilon}{\rho_o}\right]^{1/3} \qquad (C\,40)$$

from the definition of indicated air speed,

$$IAS = \sqrt{\rho/\rho_o}\, U_o . \qquad (C\,41)$$

Substituting Eqs. (C39), (C40), and the expression for p , Eq. (C26) into Eq. (C37) we find

$$\sigma_g = \frac{(4\pi)^{1/3}}{\sqrt{3}} \sqrt{C_2}\, \rho_o^{2/3} g^{-1/3} \left(\frac{W}{S C_{L_\alpha}}\right)^{-2/3} \left(\frac{\rho}{\rho_o}\right)^{-1/6} (IAS) R \sqrt{f(X_1)} \qquad (C\,42)$$

or

$$\sigma_g = K_1 (IAS)\, R \qquad (C\,43)$$

Now K_1 is directly a function of the aircraft wing loading parameter, $W/S\, C_{L_\alpha}$, and density. These two parameters have another effect on K_1 in that combined with k_1 (the wave number below which the turbulence spectrum is assumed flat) they define X_1 .

The variation of K_1 with $W/S\, C_{L_\alpha}$, ρ , and k_1 can be considered in two parts. The value of K_1 for $k_1 = 0$ (no flattening of turbulence spectrum) plus a correction factor for $k_1 \neq 0$, i.e.,

$$K_1 = (K_1)_{k_1 = 0} \left[\frac{K_1}{(K_1)_{k_1 = 0}}\right] \qquad (C\,44)$$

From Eq. (C38) we find that (if $k_1 = 0$, $X_1 = 0$)

$$f(0) = \pi/\sqrt{3} \tag{C 45}$$

Therefore

$$(K_1)_{k_1 = 0} = 2^{2/3}\, 3^{-3/4}\, \pi^{5/6} \sqrt{C_2}\, \rho_o^{2/3}\, g^{-1/3} \left(\frac{\rho}{\rho_o}\right)^{-1/6} \left(\frac{W}{S\, C_{L_\alpha}}\right)^{-2/3} \tag{C 46}$$

Using a mixture of metric and English units such that the following parameters have the indicated units

$\frac{W}{S\, C_{L_\alpha}}$	lb/ft^2
K_1	$\frac{sec}{m^{2/3}\ knots}$
IAS	knots
R	$\frac{m^{2/3}}{sec}$

then Eq. (C46) can be written setting $C_2 = 0.15$

$$(K_1)_{k_1 = 0} = 0.01462 \left(\frac{\rho}{\rho_o}\right)^{-1/6} \left(\frac{W}{S\, C_{L_\alpha}}\right)^{-2/3} \tag{C 47}$$

A plot of Eq. (C 47) is given in Fig. C 1.

The correction for $k_1 \neq 0$ is only a function of X_1, i.e.,

$$\frac{K_1}{(K_1)_{k_1 = 0}} = \sqrt{\frac{f(X_1)}{f(0)}} = \frac{3^{1/4}}{\sqrt{\pi}} \sqrt{f(X_1)} \tag{C 48}$$

where from Eq. (C 36)

$$X_1 = \frac{4\pi k_1}{g\rho} \frac{W}{S\, C_{L_\alpha}} = 2\pi \frac{k_1}{pU_o}$$

A plot of Eq. (C 48) is given in Fig. C 2.

3. Typical Values of K_1

To obtain an appreciation for typical values of K_1 and variations of K_1 with flight condition, sample calculations were made for four aircraft: Cessna 180, Beech 65-90 King Air, Lockheed T-33A, and Boeing 707-420. For the first three aircraft the calculations were made for typical weights. For the 707

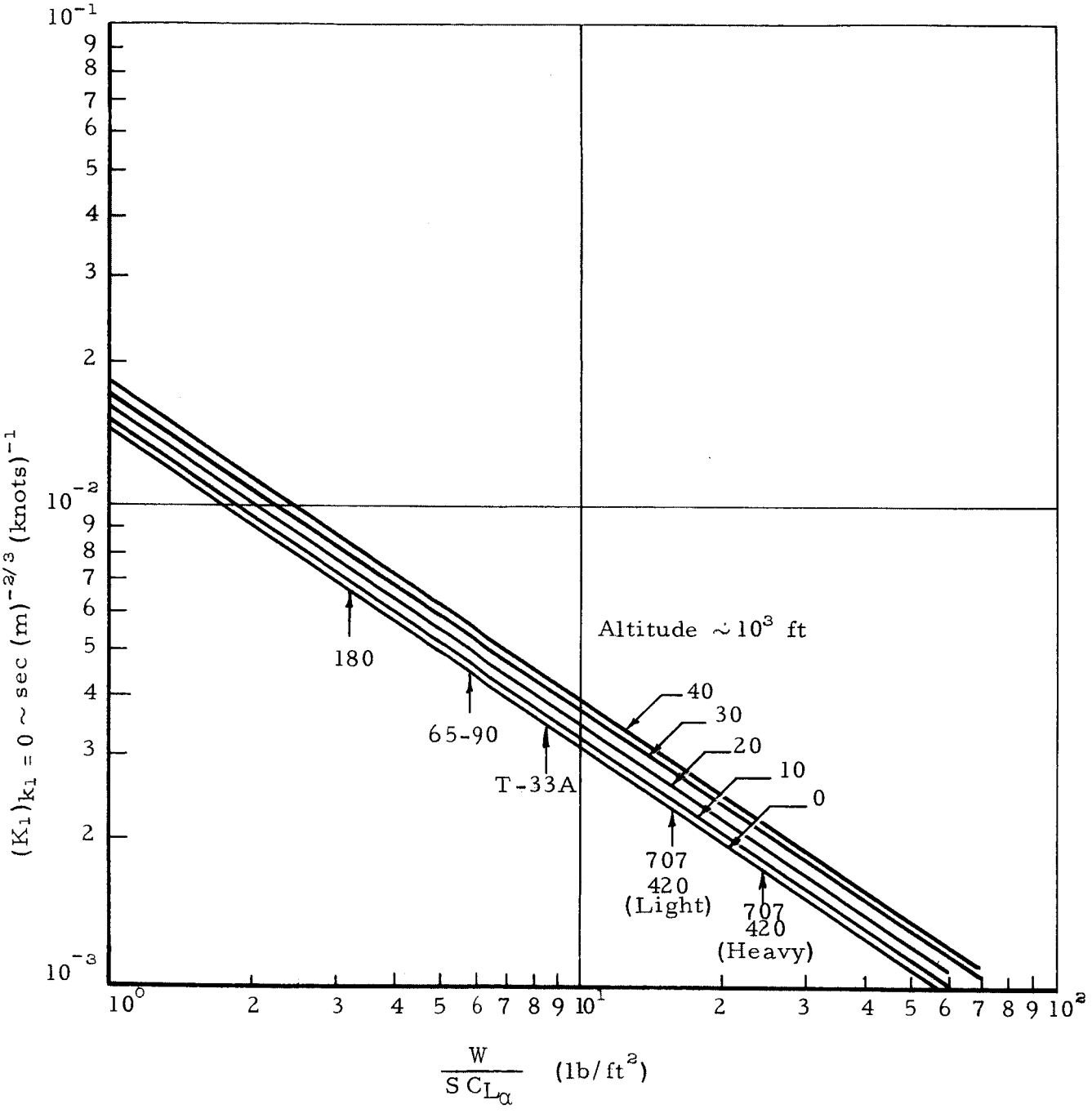

Fig. C1. $(K_1)_{k_1 = 0}$ Versus $\frac{W}{S C_{L_\alpha}}$ for Various Altitudes and Aircraft

Empirically Fitted Curve $\frac{K_1}{(K_1)_{k_1 = 0}} = 1 - 0.111x + 7.7 \cdot 10^{-3} x^2$

where $x = \frac{W}{SC_{L_\alpha}} \cdot \frac{4\pi k_1}{g \rho_{20,000\ ft}}$ with g in ft sec^{-2}

and ρ in slugs ft^{-3} agrees with indicated points within 1%.

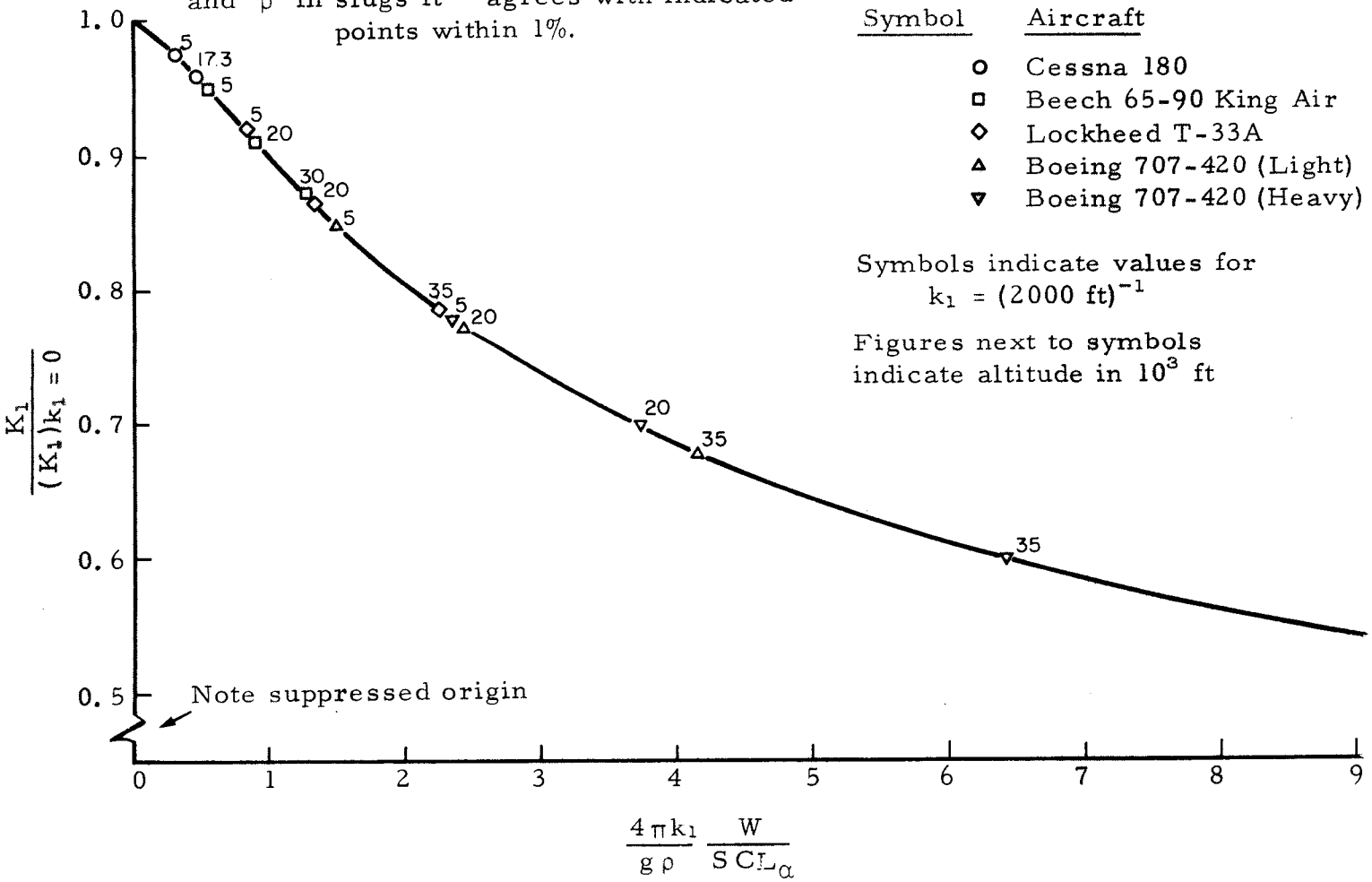

Fig. C2. Effect of Flattening the Turbulent Spectrum at $k_1 = (2000\ ft)^{-1}$

Table C1

AIRCRAFT SURVEY

Aircraft	Weight (lb)	$\frac{W}{S C_{L_\alpha}}$ (lb/ft^2)	Altitude (ft)	$(K_1)_{k_1 = 0}$ $\left[\sec (m)^{-2/3} (\text{knots})^{-1}\right]$	X_1 for $k_1 = (2000 \text{ ft})^{-1}$	K_1 for $k_1 = (2000 \text{ ft})^{-1}$ $\left[\sec (m)^{-2/3} (\text{knots})^{-1}\right]$
Cessna 180	2,600	3.25	5,000	0.00684	0.310	0.00666
			17,300*	0.00730	0.456	0.00700
Beech 65-90 King Air	7,400	5.8	5,000	0.00464	0.554	0.00441
			20,000	0.00504	0.894	0.00459
			30,000*	0.00534	1.27	0.00465
Lockheed T-33A	12,000	8.5	5,000	0.00360	0.810	0.00331
			20,000	0.00390	1.31	0.00339
			35,000	0.00427	2.25	0.00336
Boeing 707-420	180,000	15.6	5,000	0.00239	1.49	0.00203
			20,000	0.00259	2.40	0.00201
			35,000	0.00284	4.14	0.00193
	280,000	24.2	5,000	0.001788	2.31	0.001398
			20,000	0.001940	3.73	0.001352
			35,000	0.002125	6.41	0.001280

*Service ceiling for this aircraft

the calculations were done for both a light weight condition and for 90 per cent of maximum take-off weight.

A key parameter in the K_1 calculations is the wing loading parameter $W/S\,C_{L_\alpha}$. If aerodynamic data for the lift curve slope, C_{L_α}, is not available it can be estimated by the method of reference 6, i.e.,

$$\frac{C_{L_\alpha}}{c_{1_\alpha} \cos \Lambda} \doteq \frac{F}{\sqrt{4 + F^2} + 2} \qquad (C\,49)$$

where

$$F = \frac{2\pi A}{c_{1_\alpha} \cos \Lambda} \qquad (C\,50)$$

A = wing aspect ratio (span^2/area)

c_{1_α} = lift curve slope of a wing section perpendicular to quarter-chord line at a Mach number equal to $M \cos \Lambda$, per radian

M = free-stream Mach number

Λ = angle of sweep of quarter-chord line

The value of K_1 for the example aircraft were computed for both k_1 equal zero and $(2000\ \text{ft})^{-1}$ and at altitudes from 5000 to 35,000 ft. The results are listed in Table C1. The most significant result of these calculations is that altitude effects on K_1 are relatively minor. Setting K_1 to the value for an average altitude, say 20,000 ft, would only introduce maximum errors of 10 per cent. With this simplication the only aircraft parameter which affects K_1 is $W/S\,C_{L_\alpha}$.

D. Human Factor Aspects, σ_h Versus R

Experimental data has shown that human subjective opinion of vibration environments depends not only on the magnitude of the accelerations experienced but also on the frequency of the oscillations. The experimental data of reference 7 covers the frequency range from 1 to 28 cycles per second. These data show that for the levels rated extremely annoying and alarming, the

subjects were much more sensitive to oscillations at 1 cps than any other frequency tested. This suggests that a useful measure of subjective opinion for a person flying through turbulent air might be the acceleration level for frequencies near 1 cps. Other evidence presented by reference 7 suggests that frequencies near 5 cps may also be of particular importance in determining the human evaluation of severity of turbulence. Which frequency is chosen for calculation will not change the functional form of the relationship between the human response evaluation factor, σ_h, and R, although it will change the value of the constant of proportionality. It should be noted that any of the frequencies mentioned above relate to wave lengths well within the inertial subrange, and therefore the initial turbulent spectrum given by Eq. (C1) can be used in any derivation without concern for where the spectrum may level off.

Assuming that a human's subjective opinion depends primarily on the magnitude of the accelerations at one frequency, ω_h, then the severity of the aircraft motion, σ_h, for a rigid aircraft is proportional to

$$\sqrt{G(\omega_h)} \left| \frac{\ddot{z}}{w_g} (\omega_h) \right| \tag{C51}$$

The constant of proportionality will depend on the location of the pilot or passenger with respect to the center of gravity of the aircraft.

$$\sigma_h \sim U_o^{1/3} \epsilon^{1/3} \frac{p}{\sqrt{\omega_h^2 + p^2}} = \frac{U_o^{1/3} \epsilon^{1/3}}{\sqrt{1 + (\frac{\omega_h}{p})^2}} \tag{C52}$$

$$\sigma_h \sim \frac{U_o^{1/3} \rho^{-1/3} R}{\sqrt{1 + (\frac{\omega_h}{p})^2}} \sim \frac{(IAS)^{1/3} \rho^{-1/3} R}{\sqrt{1 + (\frac{\omega_h}{p})^2}} \tag{C53}$$

But, from Eq. (C26)

$$\frac{\omega_h}{p} = \frac{2 \omega_h}{g \rho U_o} \frac{W}{S C_{L_\alpha}} \tag{C54}$$

Values of ω_h/p for the aircraft and altitudes studied in Table C1 vary from 2.01 for the Cessna 180 at maximum speed at sea level to 19.5 for the heavy 707 at 35,000 ft at 450 K. Even for $\omega_h/p = 2$, the approximation

$$\sqrt{(\frac{\omega_h}{p})^2 + 1} \doteq \frac{\omega_h}{p} \tag{C55}$$

can be used with less than 10 per cent error, with the error less for larger values of ω_h/p, and so this approximation is valid for our purposes. Then

$$\sigma_h \sim (IAS)^{1/3} \rho^{-1/2} R \cdot p \tag{C56}$$

$$\sigma_h \sim (IAS)^{1/3} R \rho^{-1/2} \rho U_o \left(\frac{W}{S C_{L_\alpha}}\right)^{-1} \tag{C57}$$

and, finally

$$\sigma_h \sim (IAS)^{4/3} \left(\frac{W}{S C_{L_\alpha}}\right)^{-1} \cdot R \tag{C58}$$

APPENDIX D

T - 33 INSTRUMENTATION POD PROGRAM

A. Introduction

To obtain operational experience with the system, a T - 33 jet-trainer was made available as a platform to explore a variety of atmospheric environments. An instrument package consisting of a prototype UITS along with sensors for local static pressure, total temperature, vertical acceleration,, and q was assembled with an appropriate miniature oscillograph recorder. This equipment was built inside a detachable pod for mounting to the lower fuselage aft the wing trailing edge. A small control panel was provided for the observer in the rear cockpit. In addition to controlling such functions as instrument calibration and deicing, this panel mounted readouts for total temperature and R.

The aircraft was based at the NASA Flight Research Center, Edwards Air Force Base, California. Flights were made at selected altitudes varying from the surface to the tropopause. Turbulence when located was probed repeatedly at various speeds. In this geographic region, light to moderate turbulence was consistently found to 24,000 feet. Flights were conducted into light icing and heavy rain conditions.

B. Description of Equipment

The Universal Indicated Turbulence System, Model #2020, consisted of four components: a pitot-static tube, a sensitive fast-response differential pressure transducer, a solid state signal converter, and an appropriate panel indicator.

1. Pitot-static Tube

The unit as supplied in this instance used a Type D-1 pitot-static tube (Spec, No. AN-T-1) with 24-volt deicer heater. The tube was mounted on the baggage pod adjacent to the electronic assembly. Hence the volume and length of the lines to the differential and absolute pressure transducers were held to a minimum. With this position there would obviously be errors in pressure readings with respect to true free stream values; however, such differences were considered acceptable for the purpose of the demonstration.

2. Differential Pressure Transducer

The differential pressure transducer was a high quality variable reluctance type manufactured by Pace Engineering Company. The full range of this instrument was 0-5 psi for the first two flights and for subsequent flights the diagram was changed to give a range of 0-3.5 psi. The electrical output was nominally 0 to 5 volts, and in order that this should vary linearly with indicated air speed rather than Δp, circuitry was built in to modify this output to follow the equation

$$\text{Output volts} = 5.34\sqrt{\text{pressure PSI}} - 4$$

At the low speed end this relationship was not maintained but the signal was biased on the differential pressure board so that the output to the turbulence signal converter and the air speed galvanometer channel was correctly related at indicated airspeeds above 180 K.

The voltage output was recorded directly by the oscillograph and also analyzed by the turbulence signal converter according to the theory described in detail in Appendix B. The output voltage was directly related to the indicated air speed of the aircraft. This voltage was fed to a standard MRI Universal Turbulence System module which alters the gain of the incoming ac signal as a function of the -1/3 power of the incoming mean signal by putting the total incoming signal through a shaping circuit having a $(\text{voltage})^{2/3}$ function. The combination of the square root function in the transducer and the 2/3 function in the UTS module gives the 4/3 power of indicated air speed corresponding to the 2/3 power of differential pressure which is needed to give the final gain adjustment of the ac signal so that the final instrument output is R. The output from the signal converter was fed to an indicator in the rear cockpit and also to the oscillograph through an appropriate attenuation and calibration network. Two full scale ranges were provided.

3. Additional Instrumentation

As the static pressure sensed by the probe could be considerably in error due to its position the absolute value of the static pressure was recorded on the oscillograph. The transducer was a Kollsman type 1709-01 absolute pressure gauge.

The temperature probe was of the Franz type with a Balco wire sensing element arranged so that its resistance varied in proportion to the stagnation temperature of the air stream. The output of a temperature probe was recorded on the oscillograph and also displayed by a meter on the rear cockpit panel. The recovery factor was better than 0.98 and the response was of the

order of several seconds. The temperature range was set to cover from -60F to +40F.

To correlate between the turbulence reading R and the vertical acceleration of the aircraft an accelerometer was installed. This was basically a potentiometer type with ± 3G range and a natural frequency of about 30 cps. The sensitivity of the recording galvanometer was, however, set to read full scale in the range 0 to +2G vertical acceleration.

The oscillograph recorder was a fourteen-channel Midwest with a capacity of 150 ft of 3-5/8 wide paper. This particular recorder was the only one which was immediately available, small enough to mount in the pod, and compatible with the aircraft power system. It is designed for operation in unpressurized aircraft. Photo recording paper was used rather than film since the resolution was adequate and the extra capacity obtainable with the thinner paper was very desirable. Any one of ten different film speeds could be selected on the ground. Most of the records were run at 19 in. per minute which gave a useful run time of 90 minutes and an ultimate trace resolution in excess of 20 cps.

All control functions as well as indication of turbulence and total temperature were located on a small control panel in the radio console of the aft cockpit. The complete electronic package including transducers and the recorder was mounted as an integral unit, with the pressure and temperature probes, on a pull-out tray supported on rollers. In this way the entire unit could be removed from the pod and bench calibrated. In order to avoid thermal drift problems, the electronic package and transducers were built into a thermostatically controlled oven. Power was routed first to the control panel, then through separate circuit breakers to the recorder, to the instrumentation power supplies and finally to the pitot deicer. A block diagram of the system is shown in Fig. D1. Figures D2, D3, D4, and D5 are views of the pod on the aircraft, the tray extended for service, the mounted control panel, and the pod interior, respectively.

C. Operational Evaluation

The T-33 series of tests were primarily intended to be an operational evaluation of the UITS concept in a wide range of flight environments. About forty hours of flight time were accumulated at all flight levels from the surface up to 40,000 feet in clear air, cloud, icing conditions, and in light and heavy precipitation. From the surface to a flight level of 14,000 ft the source was primarily convective, and from 14,000 to 25,000 ft the source was either the roll portion of the lee wave in the Owens Valley or cumulus build-ups over the coastal range. No severe turbulence was found on any flight. The condition most frequently encountered was light to moderate with occasional moderate turbulence.

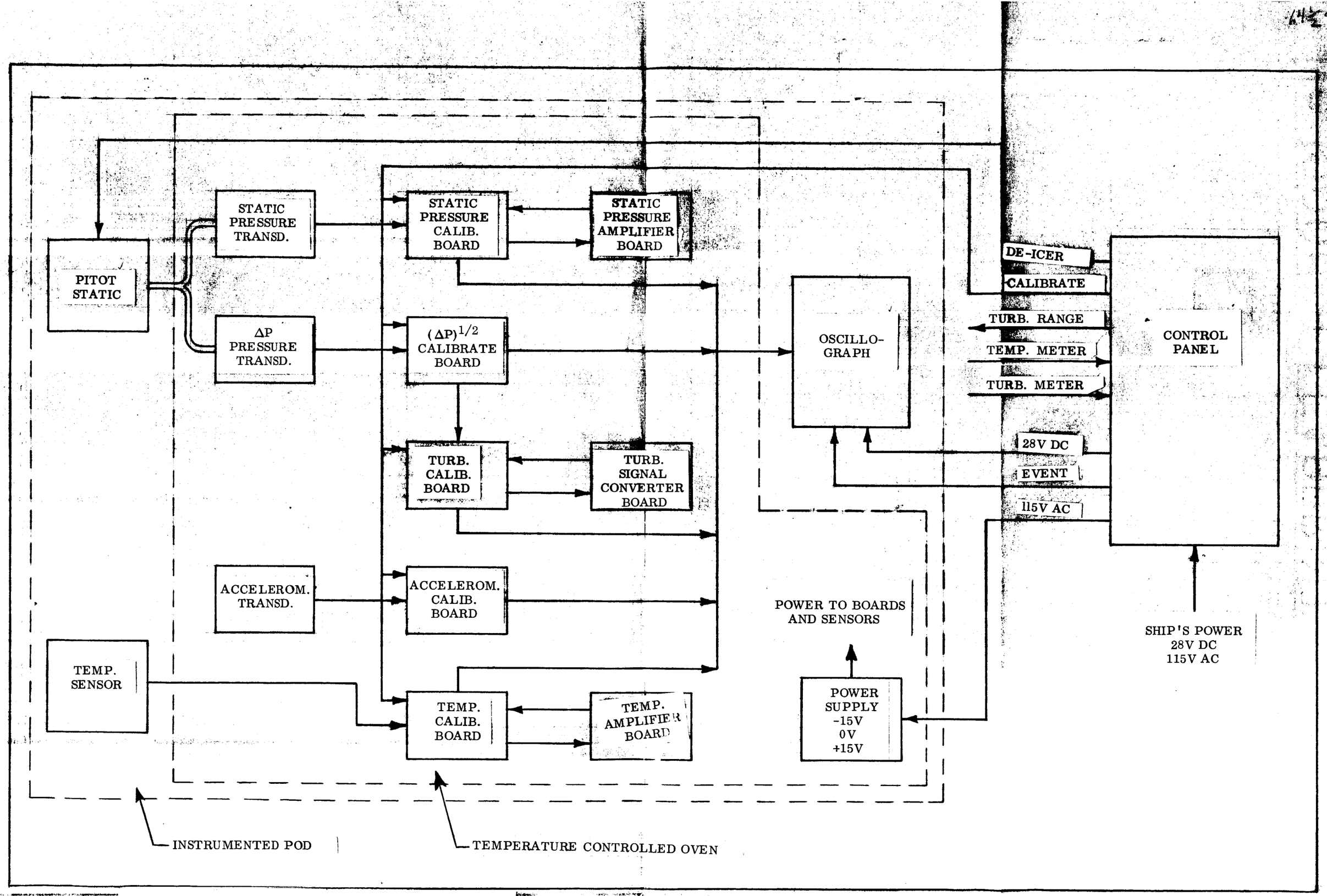

Fig. D1. T-33 Package Block Diagram

CONTROL PANEL

DE-ICER

CALIBRATE

TURB. RANGE

TEMP. METER

TURB. METER

±8V DC

EVENT

115V AC

SHIP POWER

OSCILLO-

STATIC PRESSURE AMPLIFIER

STATIC PRESSURE CALIB. BOARD

STATIC PRESS. TRANS.

PITOT STATIC

(ΔP) CALIBRATE BOARD

ΔP PRESSURE TRANS.

TURB. SIGNAL CONVERTER

TURB. CALIB. BOARD

ACCELEROM. TRANSD.

POWER TO BOARDS AND SENSORS

POWER SUPPLY +15V 0V -15V

TEMP. AMPLIFIER BOARD

TEMP. CALIB. BOARD

TEMP. SENSOR

TEMPERATURE CONTROLLED OVEN

STATIC PO

Fig. D1.

NASA

E-13424

Fig. D2. The Pod Under the T-33

NASA Flight Research Center
Edwards, California

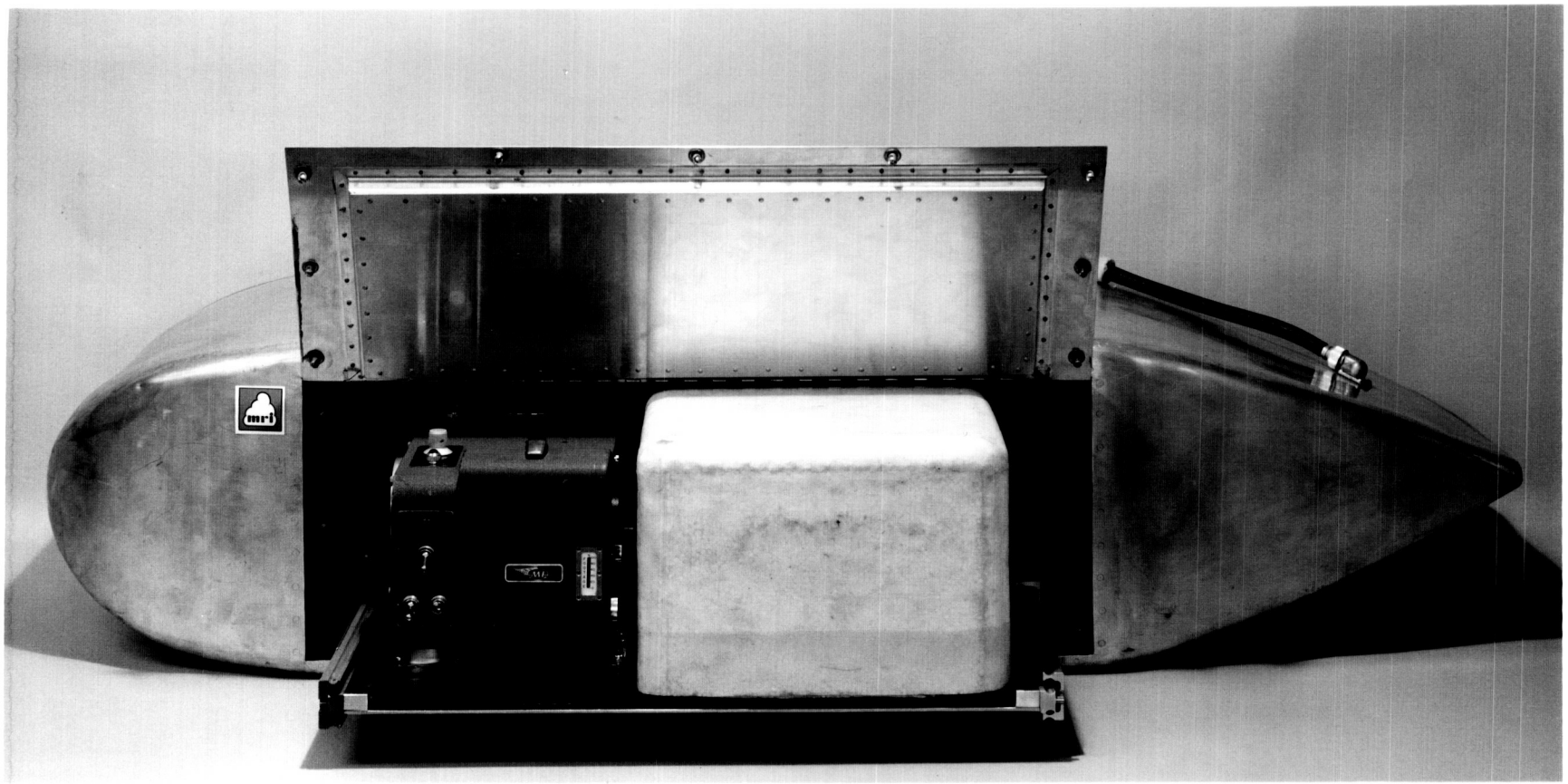

Fig. D3. Pod Tray Extended

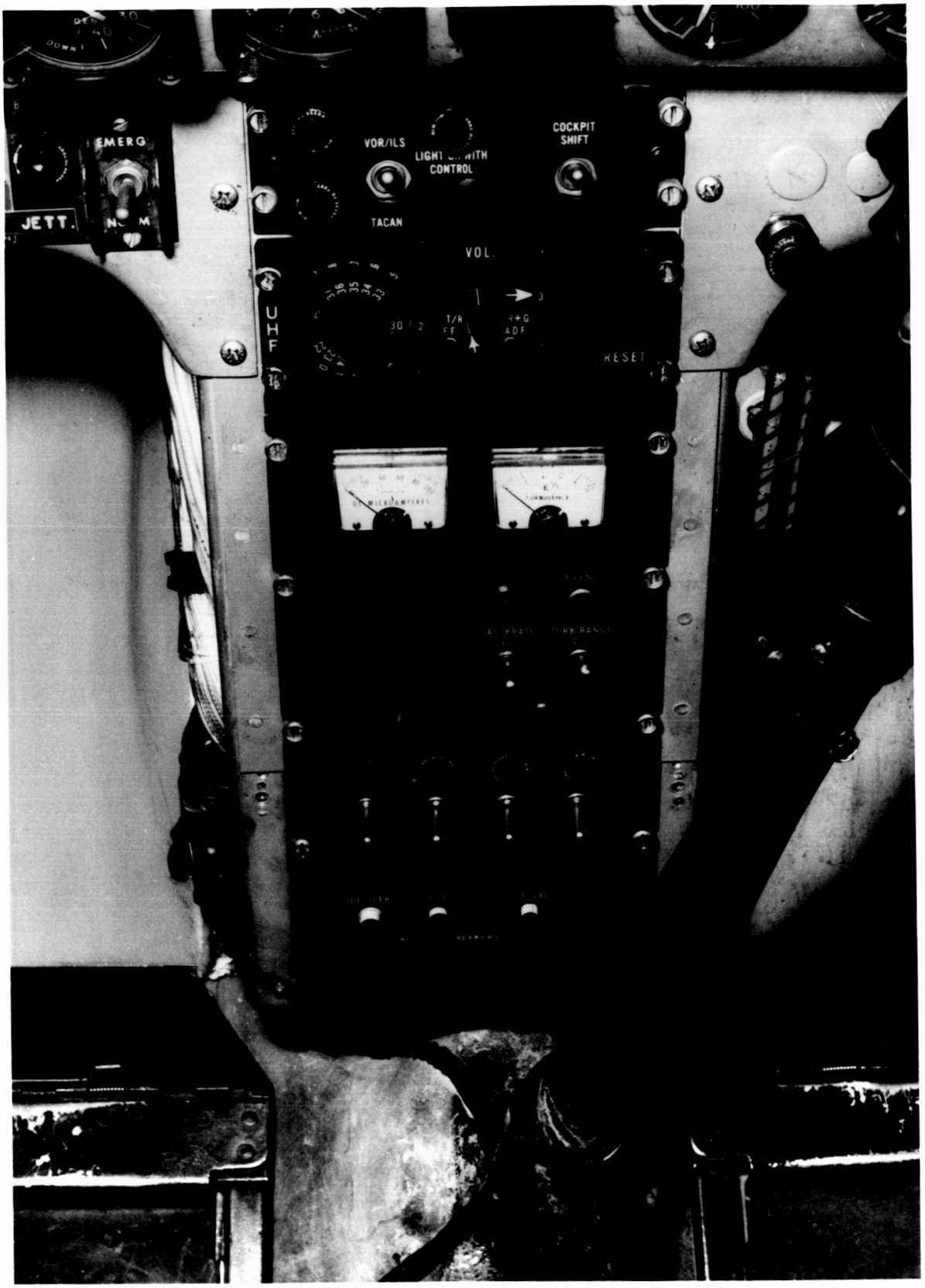

NASA
E-14200

NASA Flight Research Center
Edwards, California

Fig. D4. Control Panel in Rear Cockpit of T-33

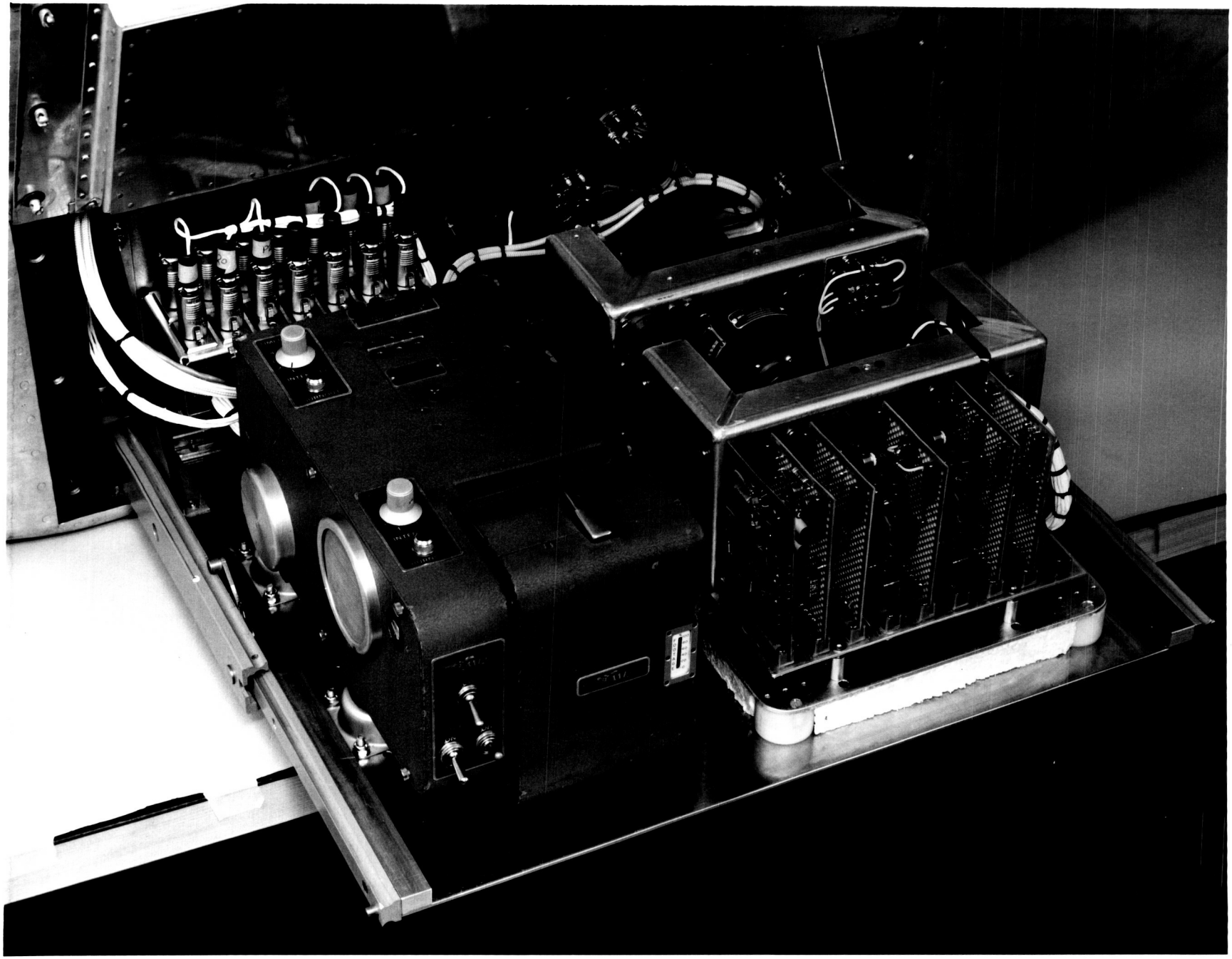

Fig. D5. Pod Interior View

During the flights the aircraft was yawed as far as possible in each direction at high, low, and medium speeds at representative altitudes up to 40,000 ft in smooth and rough air. In some cases at extreme angles the static pressure was seen to increase and a small spurious turbulence signal was induced. This effect was very probably caused by a turbulent disturbance from the pod enveloping the static orifice on the probe. Such an effect was anticipated and is the result of the mounting scheme employed.

Further experience under adverse weather conditions was desired. Light, moderate, and heavy rain was penetrated at 10,000 ft under clouds based at 11,000 to 12,000 ft. During heavy rain in smooth air the turbulence intensity indicator was observed to read zero. In moderate to heavy rain with light and light-to-moderate turbulence the readings were 0.5 to 1.0 and 1.0 to 1.5, respectively. During the course of other flights which were conducted in light icing conditions, the pitot deicer was activated and no effect was observed in the measurement of turbulent intensity.

Some difficulty was found in finding turbulence at flight levels above 25,000 ft. Below this level turbulent areas of different origins were repeatedly penetrated.

In Fig. D6, σ_g, the standard deviation of the recorded vertical accelerations, divided by R, has been plotted against IAS, the indicated air speed.

In the relationship, $\sigma_{g/R} = a(IAS)^n$, it is indicated that the power of n lies about 1. The range of the transducer which was used to obtain $\Delta p^{1/2}$ for the first two flights was changed from 0-5 psi to 0-3-1/2 psi from flight #3 onwards. R values at flight speeds below 180 K have some error because of the limitations in the pressure transducer linearizing mentioned earlier, but the effect on R is estimated to be only about 10% at 150 K. Consequently, a data point at 150 K is included in Fig. D6. The values for σ_g used in the calculations were obtained from the peak-to-peak acceleration record. During the corresponding interval, mean values of R for a six-second period were estimated; these in turn were averaged over the one-minute interval. In general, the experimental data are not consistent with the governing relationships, but the data are few and, with the anticipated scatter, cannot in themselves show the exact nature of the relationships.

The pilot's and observer's qualitative on-the-spot assessments of turbulence were recorded in the various observer's notes during nine of the T-33 flights. The corresponding R and IAS data were obtained from the chart records for the periods when the notes showed "moderate" turbulence, "light-to-moderate," etc. The airspeed range was not great and the scatter of the data points for each turbulence category (as plotted on an R versus IAS log-log

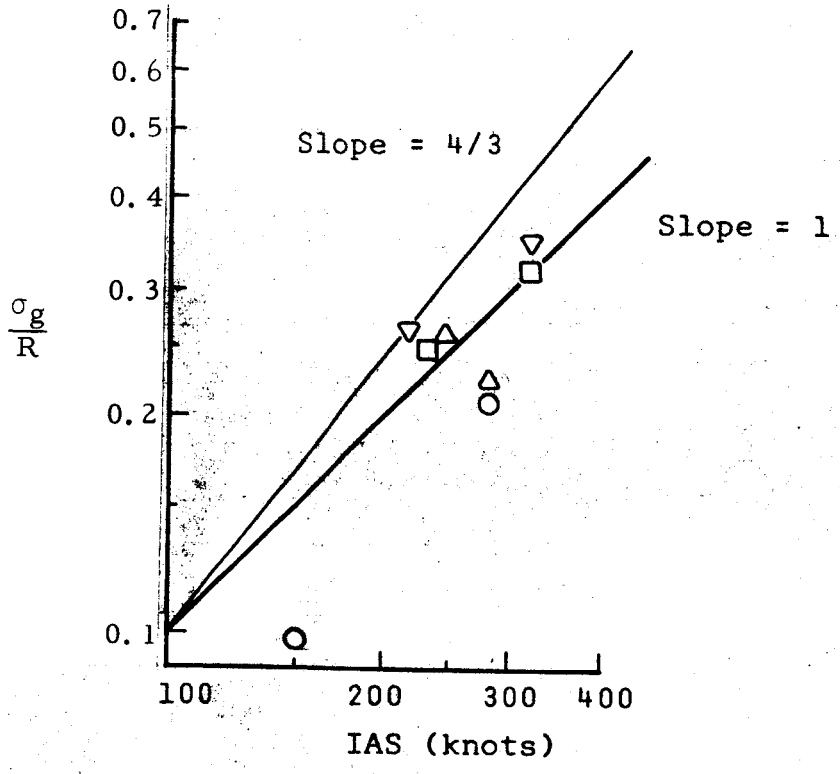

△ - Early transducer flight #1 (surface)

○ - Modified transducer flight #5 (24, 000 ft)

□ - Modified transducer flight #7 (10, 000 ft)

▽ - Modified transducer flight #14 (10, 000 ft)

Fig. D6. σ_g/R VERSUS IAS

plot) was fairly large, and so these data could not be used to verify the functional relationships represented by Eqs. (2) and (8). However, the points did stratify reasonably well in terms of the pilot and observer labels. The best-fit line representing Eq. (2) for each category gave the following values in Table I (here normalized so that K(IAS)R = 10 for the "moderate" label case).

Table D 1

TURBULENCE EVALUATION OF THE FLIGHTS

Pilot's Description		No. of Obs.	Best Fit K(IAS)R
VVL	Very very light	3	0.1
VL	Very light	5	1.0
L	Light	8	2.5
LM	Light to moderate	8	5.4
M	Moderate	7	10.0

"Moderate" was the most severe situation encountered during the T-33 program. On the log-log plot of R versus IAS the categories were rather distinct, with no overlap of the M points to the LM best-fit line, no overlap of the LM points to the L or M line, and just slight overlap of the L points beyond the VL and LM line. The few VVL points were far from the VL line.

If from Table D 1 we equate K(IAS)R to σ_h , we see that the T-33 data show σ_h to be decreased by a factor of 4 between the "moderate" and "light" categories, and to be down by a factor of 10 to 100 between "moderate" and the two categories which can be termed "negligible" ("very light" and "very very light"). In Table 3, page 9 the lower portion of the assumed σ_h scale, based on other information was given as

Title	σ_g units (assumed proportional to σ_h)
Negligible	< 0.025
Light	0.025 - 0.06
Moderate	0.06 - 0.15

It can be seen that the assumed scale is not inconsistent with the T-33 results.

D. Conclusions

The equipment proved to be quite reliable and demonstrated that the UITS did give readings which were essentially proportional to the turbulent energy of the local atmosphere and independent of the penetration speed. At any given aircraft speed, beyond the 180 K IAS minimum speed for which the Model #2020 UITS was designed, there was good agreement between the observer's qualitative evaluation of turbulent intensity and the instrument reading regardless of whether the aircraft was flying through turbulent cumulus, wave activity, or convective disturbances close to the ground. Some flights were conducted into heavy rain and light icing conditions without apparent effect on the operation of the instrument. As has been pointed out in Appendix B, the use of the straight-line approximation for turbulence signal gain control, as employed on this preliminary test version of the UITS, cannot be expected to give as much accuracy as would be found with the type of circuitry shown in Fig. B12. The test unit still satisfactorily fulfilled its role of demonstrating overall system reliability over the range of altitudes and speeds during various weather conditions, and of generating data for comparison with aircraft response and pilot evaluation information.

APPENDIX E

THE APACHE TURBULENCE SYSTEM AND ANALYSIS

A. Introduction

For this project it was deemed desirable to obtain some special turbulent spectra which could aid one in deciding on the averaging time characteristics needed in the optimum operational UITS.

The primary need is to show how the E(f) and G(f) spectra vary in time. For the UITS, the spectrum of u determines the turbulence reading while the spectrum of w determines the aircraft gust loads. For long averaging times, E(f) and G(f) should be uniquely related; in fact, then $3G(f)/4E(f) = 1$. However, for short averaging times $3G(f)/4E(f)$ will not be unity. Power spectra are ordinarily obtained representing particular intervals of time which are long enough to include at least 5 or 10 cycles of the longest period or wavelength being studied. These spectra usually show $3G(f)/4E(f)$ to be near unity. When deciding on the time constant of the optimum operational UITS, it would be valuable to ascertain how long the averaging time must be so that R , the instrument reading, really does relate to the aircraft gust load (i. e., how long must the averaging time be so that $3G(f)/4E(f)$ is mostly close to unity).

Another need relating to averaging time is to use the true turbulence signature as obtained on the tape recorder (pressure channel) as the input into the laboratory breadboard version of the UITS. Then the time constant of the UITS can be varied, and the observer can estimate which time constant seems most suitable. In effect, the tape recorder is inserted into the UITS at the output of the Pace pressure sensor, thus permitting the "flight" to be rerun as desired.

The E(f) and G(f) power spectra can also be helpful in establishing how well the UITS concept works under non-ideal conditions where isotropy and the -5/3 spectra laws are less expected: for example, when the aircraft is flying close to the ground, or just at the top of a convective layer with a strongly stable lid.

After the start of the project significant spectra from clear air turbulence (CAT) cases became available (reference 2). These spectra verified that the -5/3 spectra can be good approximations to the turbulence in CAT. The spectra are presented on Fig. E1. The -5/3 spectrum shape is evident in the data for wavelengths up to 1000 ft, and in many cases is observed to far longer wavelengths.

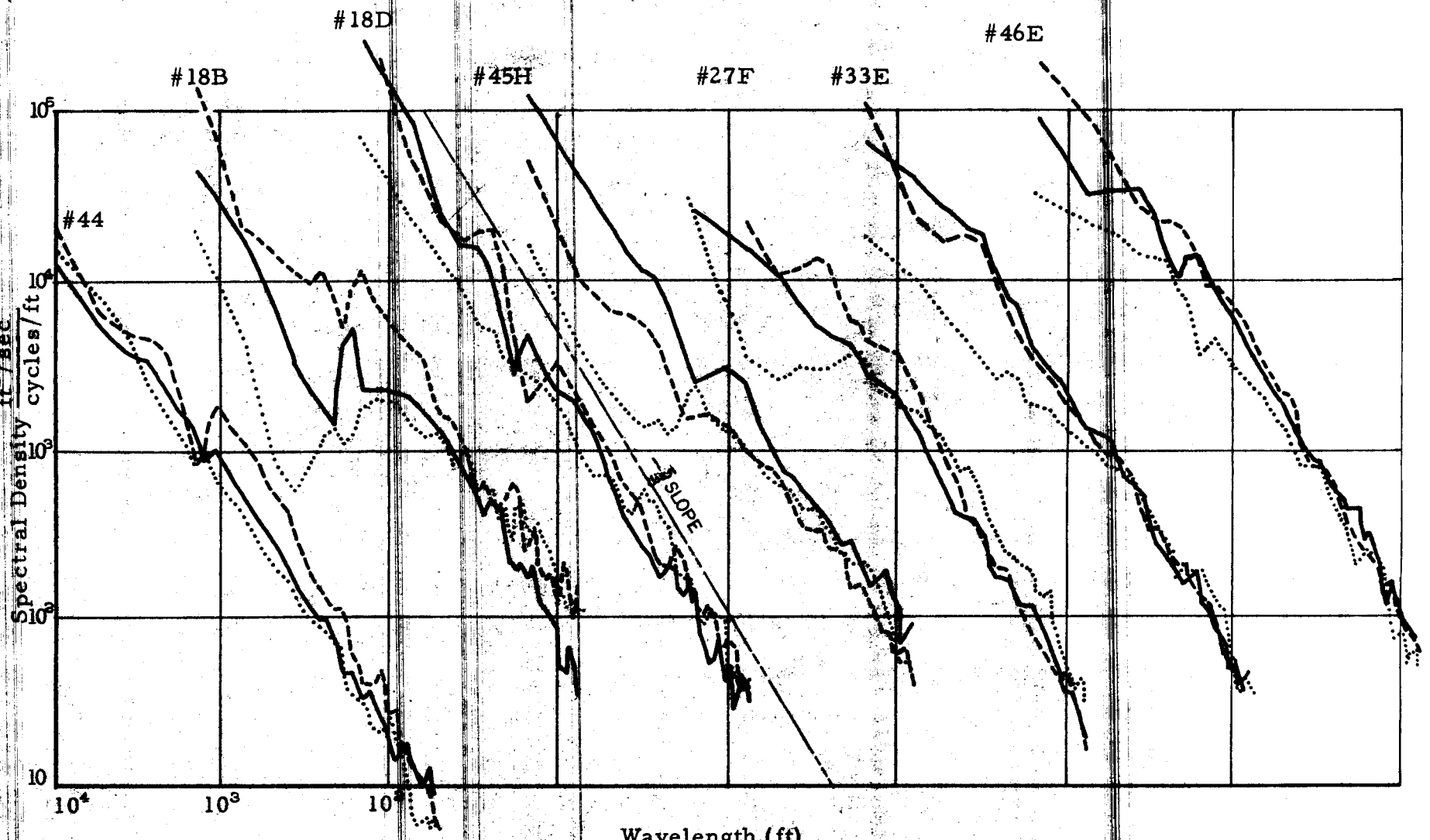

Fig. E1. CAT Spectra Obtained in Reference 2 Runs

Fig. E1. CAV Spectra Obtained in Reference

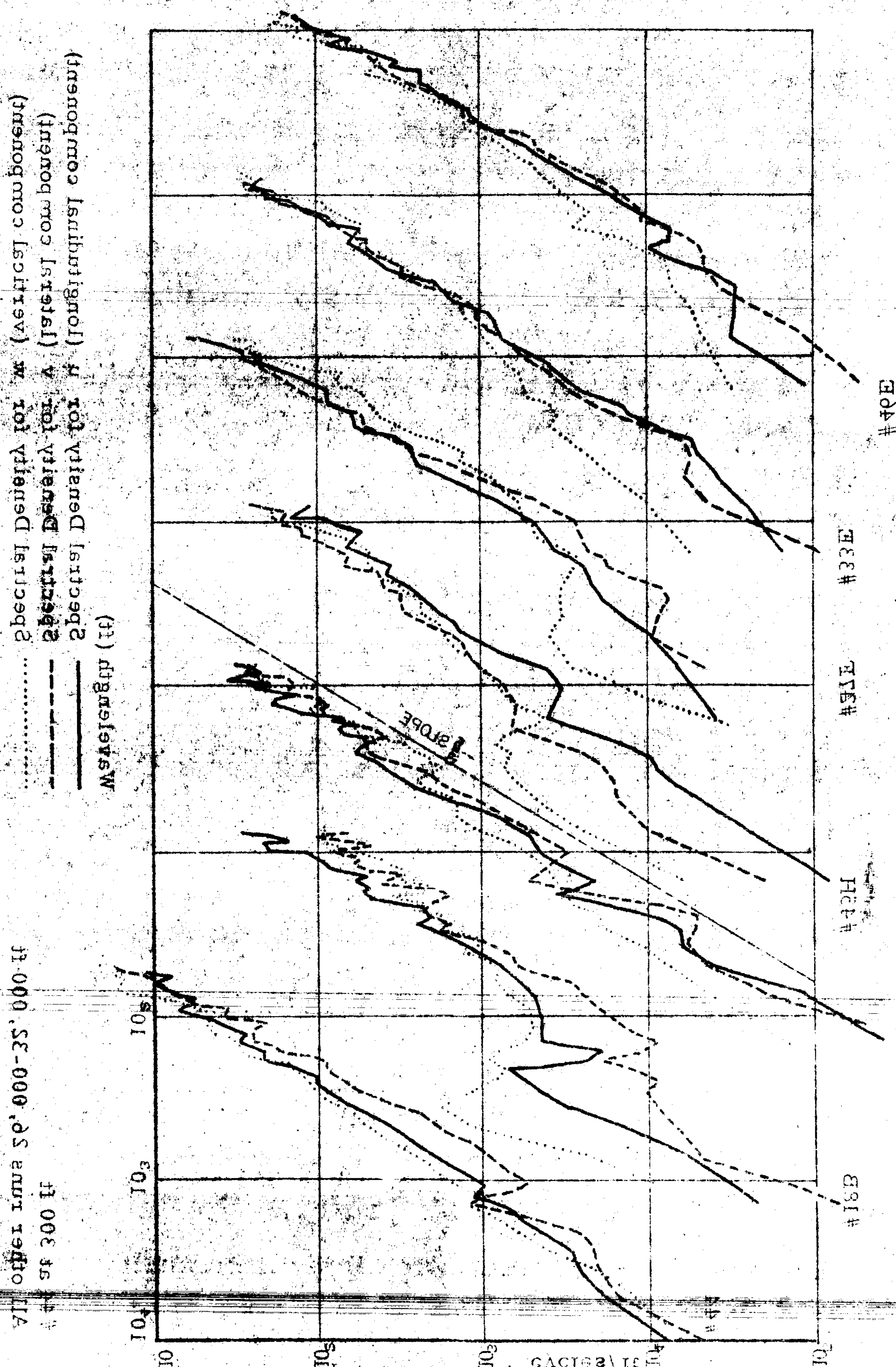

Of most importance for this project is the relation between the u spectrum in the wavelength range of approximately 20 to 200 ft (which determines R) and the w spectrum in the wavelength range 200 to 2000 ft (which determines most of the aircraft gust load, σ_g, for many aircraft). The ratio is given below for all the seven cases. It is estimated by fitting straight lines for the above ranges to the appropriate curves by eye, and taking the points from these approximations at 100 ft for the R portion and at 1000 ft for the σ_g portion.

Table E1

CAT SPECTRA DENSITY RATIOS FROM DATA OF REFERENCE 2

Run Number	$\left(\frac{G_{1400\ ft}}{E_{200\ ft}}\right)$
44	29.6
18B	23.4
18D	37.0
45H	12.7
27F	44.2
33E	33.4
46E	31.0

The ratios show fair consistency, except for the one for run 45H where the G(f) curve goes very low at wavelengths beyond 1000 feet. Since we are here most interested in σ_g/R, which is proportional to the square root of the ratio of the spectra densities given in Table E1, it is informative to take the square root and see how σ_g/R would vary. Ignoring the two extreme cases and normalizing to a mean value of 1.00, one finds the σ_g/R values to be 0.98, 0.87, 1.09, 1.04, and 1.00 (the two extreme values give 0.64 and 1.19). These show a rather small variability to the σ_g/R relationship on which the application of the UITS is based, at least for the long averaging times used in the spectra runs.

B. Measurement Technique

It was desired to get the longitudinal and vertical turbulent spectra, E(f) and G(f) from high frequencies (short wavelengths) to low frequencies (long wavelengths), with the frequency band covering the entire range of interest for either the UITS (longitudinal turbulence, about 1 to 30 cps) or for the response of the aircraft (vertical turbulence, say, 1/10 to 5 or 10 cps). The turbulence measurement of E(f) is easy to provide instrumentation for. A standard Pace pressure transducer of the type used readily operates from dc to frequencies above 100

cps, and the Apache aircraft provides a stable platform for the sensor in the longitudinal direction down to 1 cps.

The requirement for the w signal G(f) is harder to meet. A vertical direction vane can handle the high frequency requirements (the vane actually used had a response distance estimated to be about 2 feet, corresponding to a time constant of about 1/100 second). The pitching motion of the aircraft is taken into account, for all frequencies, by a pitch gyro mounted anywhere in the aircraft. The aircraft vertical motion is ascertained by integrating a vertical accelerometer in the aircraft. This introduces limitations at the low frequency end because of the accuracy of the sensor, its orientation, and the integration procedure. By limiting the lowest frequency of interest to 1/5 cps, various compromises could be made which permitted the instrumentation to be simple. The accelerometer could be rigidly mounted in the aircraft (actually near the vane so as to minimize errors). The data was only used when the plane was in steady flight, being carefully piloted to eliminate large pitching, rolling, or unsteady motions which would put errors into the accelerometer interpreted as a $\ddot{z}$ sensor. The integration was performed with a high pass filter characteristic time constant of 30 seconds. Thus w had good relative accuracy for, say, 1/5 cps frequencies and higher, although lacking absolute accuracy or accuracy at lower frequencies. Such an integration time constant makes it a far simpler job to keep the w signal within a prescribed scale during the tape playback and data assembly (whether the data are handled digitally or, as was actually done, by analog computer).

If α_1 is the angle of the air with respect to the aircraft (α_1 obtained by the vane on the instrument boom, far enough forward to avoid air flow distortion due to the aircraft), and if α_2 is the pitching angle of the aircraft, then $w_1 = U(\alpha_1 - \alpha_2)$ is the vertical velocity of the air relative to a horizontal plane through the aircraft. If the aircraft vertical acceleration $\ddot{z}$ is measured, then the vertical velocity w_2 of the aircraft is the integral of $\ddot{z}$. The vertical velocity of the air is then $w_1 + w_2$.

$$w(t) = w_1 + w_2 = U\left[\alpha_1(t) - \alpha_2(t)\right] + \int_0^t \ddot{z}\, dt \qquad (E1)$$

For the accuracy required here, U can be considered as the constant U_0 throughout a traverse. $\alpha_1 - \alpha_2$ was formed in the aircraft instrument package and put on one channel of the analog FM-FM tape recorder; thus in effect this channel gave w_1. $\ddot{z}$ is approximated by an accelerometer mounted rigidly in the aircraft. Since this variable is integrated for relatively long periods, any error in it can make an appreciable difference in the resulting w_2. For simplicity, in the analysis laboratory the $\ddot{z}$ output is given a very small d-c correction voltage as required to keep the integral value, w_2, on scale. The correction voltage is established experimentally before any spectral density runs,

and then not altered as the runs are made.

During analysis it is easy to establish the scale factor for w_1, but difficult to do for w_2. Therefore the w_2 scale factor or gain was adjusted experimentally. The aircraft was controlled to a rapid up and down motion in still air. Thus w_1 and w_2 vary while $w = 0$. The gain of the w_2 trace was varied so that $w_1 + w_2$ was a minimum. The aircraft gyrations were severe, meaning the accelerometer was sometimes not vertical, so the $w_1 + w_2$ trace cannot be expected to give exactly zero in this calibration technique. As performed, w was less than 1/10th of either w_1 or w_2.

C. Aircraft Instrumentation

The instrumented MRI supercharged Piper Apache was used for the turbulence studies. Fig. E2 shows the aircraft with the special instrument boom projecting out of the nose for this project. The other probes on the aircraft are part of the standard meteorological research package.

The special instrumentation for this project is divided into two groups: (1) the sensors which are mounted in an aluminum boom attached to the nose of the aircraft, and (2) the electronics mounted in the existing instrumentation package for processing the information received from the transducers and to provide suitable calibration voltages for the recorder. An Ampex Model SP300 tape recorder is used to record the data obtained from the boom mounted sensors.

Fig. E3 gives exterior details of the boom, the angle vane, and the pitot-static tube. Fig. E4 shows the boom interior details.

Fig. E5 is a block diagram of the whole turbulence system.

1. Air-Sensing Transducers

Three pressure transducers, Model CP51, manufactured by the Pace Engineering Company of North Hollywood, California, were mounted in line. They were connected to a common pitot-static sensor in the boom (see Fig. E3). The units provided three different dc outputs: (a) proportional to the square root of the differential pressure; (b) proportional to the differential pressure at the point of the boom; (c) proportional to the cube root of the differential pressure. The output of each was sufficient to drive the recorder directly.

Fig. E2. The Piper Apache Aircraft

Fig. E3. The Boom, Showing Angle Vane and Pitot-Static Tube

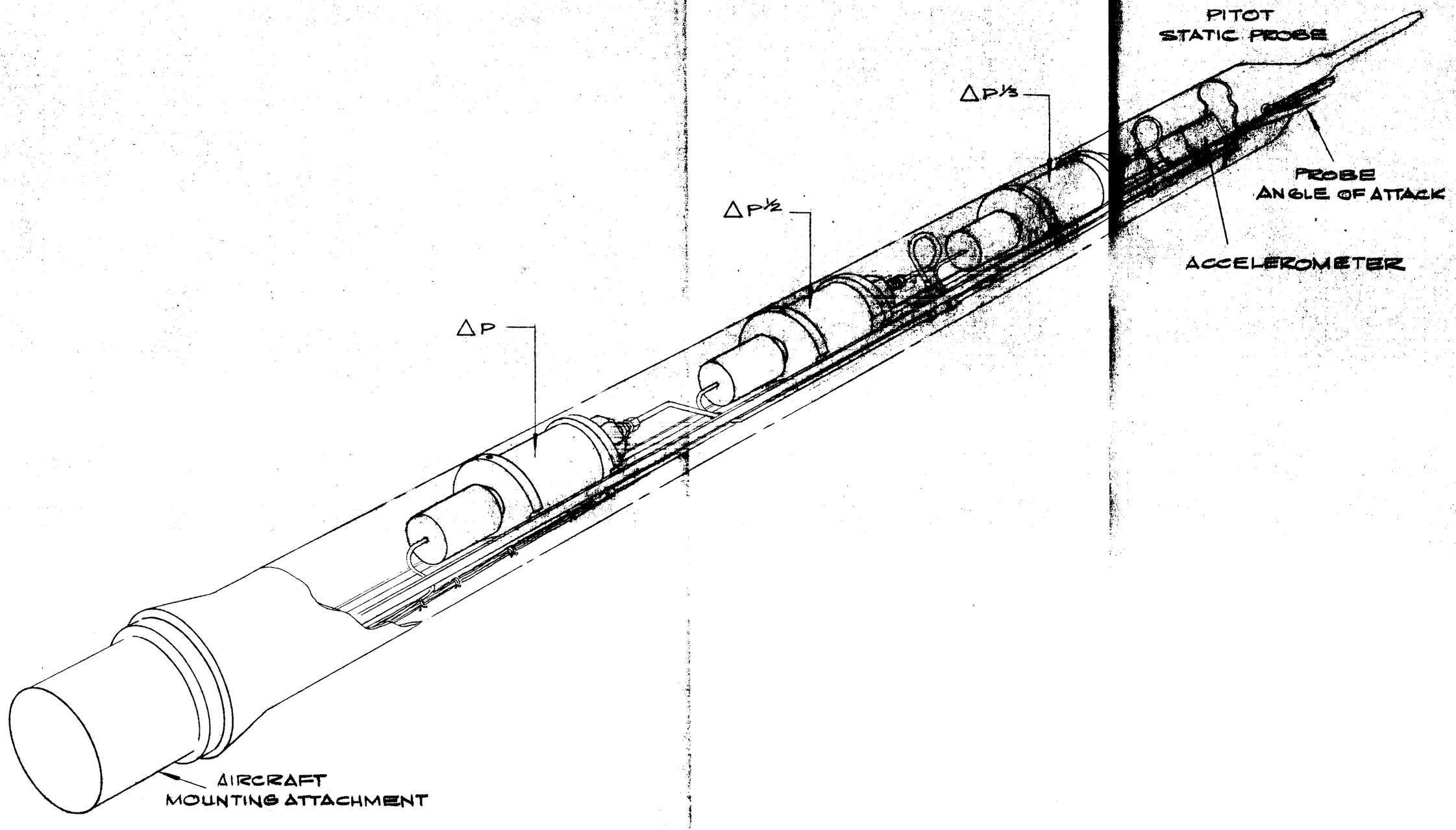

Fig. E4 Instrument Boom; Interior Details

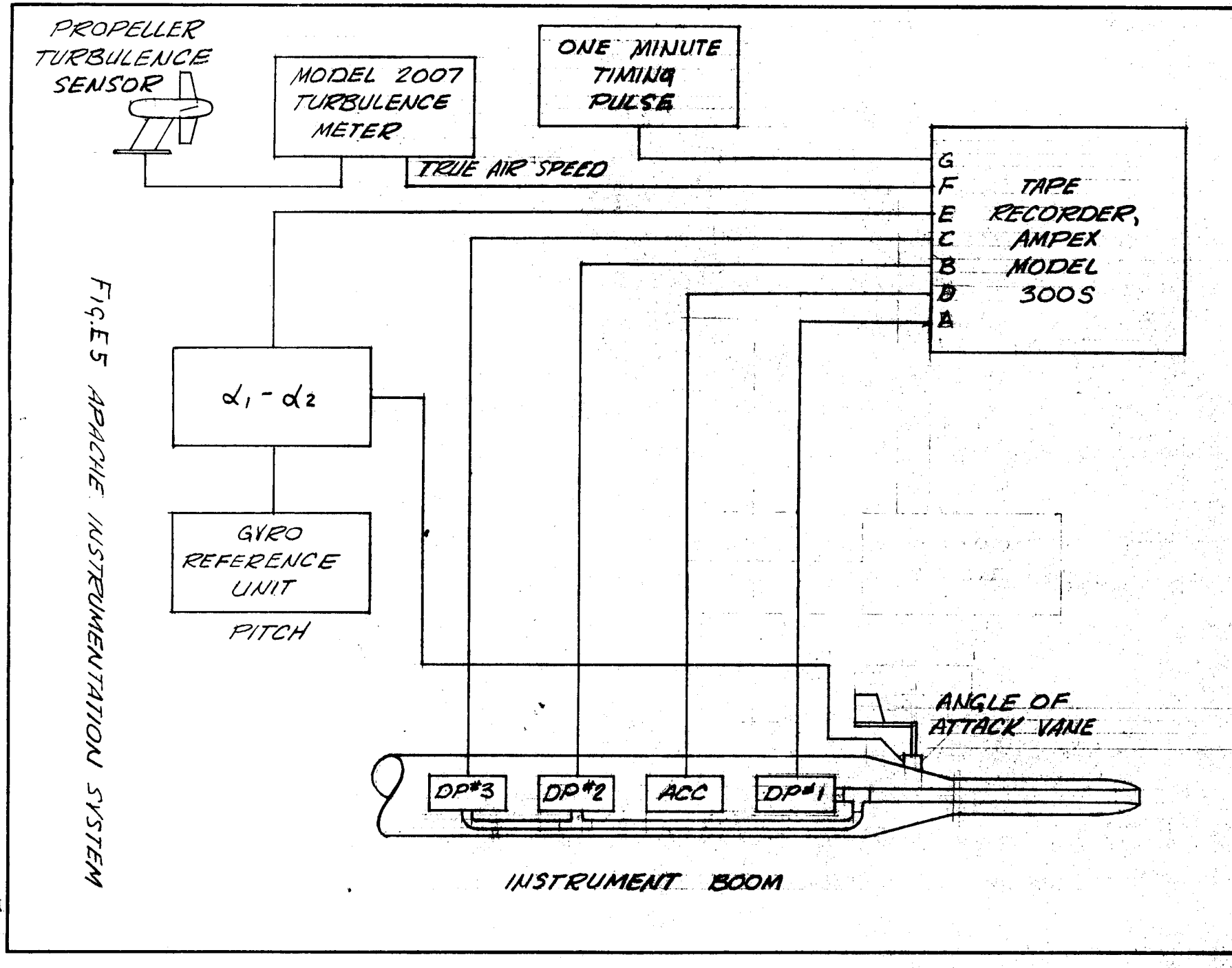

FIG. E5 APACHE INSTRUMENTATION SYSTEM

Mounted close to the point of the boom is an accelerometer also manufactured by Pace Engineering Company. The accelerometer has a high level output and the only processing required is to filter the high frequency components which are produced by vibration of the boom approximately one foot from the pressure transducer intake. The metal vertical angle vane is small, light, and designed for minimum moment of inertia. Its response distance is estimated as under two feet. The vane drives a low torque potentiometer through a 2:1 ratio gear and is limited mechanically to a maximum vane angle of approximately ± 10 degrees.

The boom section is entirely self-contained and once mechanically detached from the aircraft can be removed by withdrawing two connectors. The top connector supplies the aircraft 28 V dc for the transducers and the lower plug handles all transducer outputs.

2. Aircraft Electronics Package

The module in which the majority of the aircraft electronics is mounted contains a precision dc voltage supply from which all calibration voltages are derived. This supply is operated from the 115 V 60 cycle inverter in the aircraft, and by rectifying and regulating the output a perfectly "clean" dc is achieved isolated from all aircraft system noise. Precision resistor dividers provide the various calibration voltages required by each sensor as follows:

Pressure transducers Nos. 1, 2, and 3 calibrated at an output voltage representing 80 and 160 knots;

Accelerometer--a voltage is provided equivalent to 0 G, 1 G, and 2 G;

Angle of attack sensor--a calibration voltage is provided proportional to +5°, 0, and -5°.

A switch is provided on the front panel of the module giving three calibration positions and one operate position. At each of these points all channels are calibrated or operate directly, thus simplifying the calibration of all channels.

The angle of attack sensor is compared continuously to a gyro-stabilized potentiometer operating in the pitch mode. As a result, the voltage readout is the difference between the angle of attack and the pitch angle of the aircraft. This is a relatively low level and amplification is necessary through an

operational amplifier. This gives a full scale output of ±10° and an input voltage is provided to give a calibration at ±5°.

A control box is mounted in the electronics package for the Gyro to provide power for the run-up, erection, and caging operations.

3. Recorder

The Ampex SP300 is operated in the FM mode at a tape speed of 7-1/2 inches/second using 1/2-inch tape. Seven data channels are utilized, six for sensor outputs and one to monitor "wow" and flutter in the tape transport. The monitor channel is provided with an input from the built-in calibration voltage of the recorder; this channel is also used to record a one-minute marker pulse for correlation of data obtained from a Brush recorder existing in the aircraft. The six active data channels are as follows:

Pressure transducer No. 1
Pressure transducer No. 2
Pressure transducer No. 3
Accelerometer
Angle of attack
True air speed

A precision solid state 60-cycle inverter is used to drive the tape recorder to reduce "wow" in the capstan drive.

4. Existing Aircraft Instrumentation

A complete data system existed in the aircraft prior to the addition of the above system and this was operated throughout the flights. A Brush 6-channel recorder was used and any event notes, etc., were made on the chart; the two recorders were correlated by the one-minute time scale pulses and also by the recording of one common channel (TAS) on both recorders.

The Brush channels were as follows:

Turbulence } MRI propeller system
TAS }
Aircraft heading
Air temperature
Relative humidity

After each flight, tape data were played back onto the Brush recorder to enable appropriate sections to be selected for computer processing.

5. Analysis of Spectra, E(f) and G(f)

From the analog voltage traces u and w one can obtain power spectral densities either by analog or digital means. Analog means were selected for this project because, for the type of data presentation desired, the analog method turned out to be more economical than equivalent digital techniques by a factor of over two. The data desired were continuous plots of E(f) and G(f) for selected frequencies, to show how portions of the spectra vary over particular averaging times.

The spectral densities were obtained using a general purpose PACE TR-48 analog computer. The principles of obtaining the spectra are presented in reference 8. Fig. E6 presents a block diagram of the filtering technique. Filter #1 removes high frequencies and low frequencies, and brings the signal to a zero average. The clipping circuit eliminates the effect of an occasional noise spike. Active filter #2 constitutes the primary filter function. Three smoothing periods are used simultaneously. Eight filter frequencies are used, one for each time the tape is run: 1/6, 1/3, 2/3, 4/3, 5/2, 5, 10, and 15 cps. Representative filter characteristics are depicted in Fig. E7. It can be seen that the filter bandwidth is proportional to the center frequency.

The scales of the spectral densities of Fig. E8 are arbitrary. It is the time histories rather than the absolute values with which we are concerned here. Careful examination of the plots at the higher frequencies show that for averaging time τ = 2 seconds the individual curves are rather erratic, for τ = 30 seconds they are rather smooth, while for τ = 5 seconds they are in between. At intermediate frequencies, say, 5/2 cps, the τ = 5 seconds and the τ = 30 seconds curves are more similar. At the high frequencies the u and w spectral density curves are rather similarly shaped for τ = 30 seconds, but correlate rather poorly for τ = 2 seconds and fairly poorly for τ = 5 seconds. Considering that the UITS filter makes main use of the 3 to 10 cps range, from the above observations one would be led to feel that an instrument averaging output time constant of 6-10 seconds might be a reasonable compromise between the desire for detailed information and the desire to have the instrument reading not too erratic. For higher speed aircraft, the time constant might well be shortened. Therefore, in summary, an instrument averaging time constant in the range 6-10 seconds seems reasonable for regular versions of the UITS. The electronic package should be made to have the rise time comparable to the decay time in the instrument output.

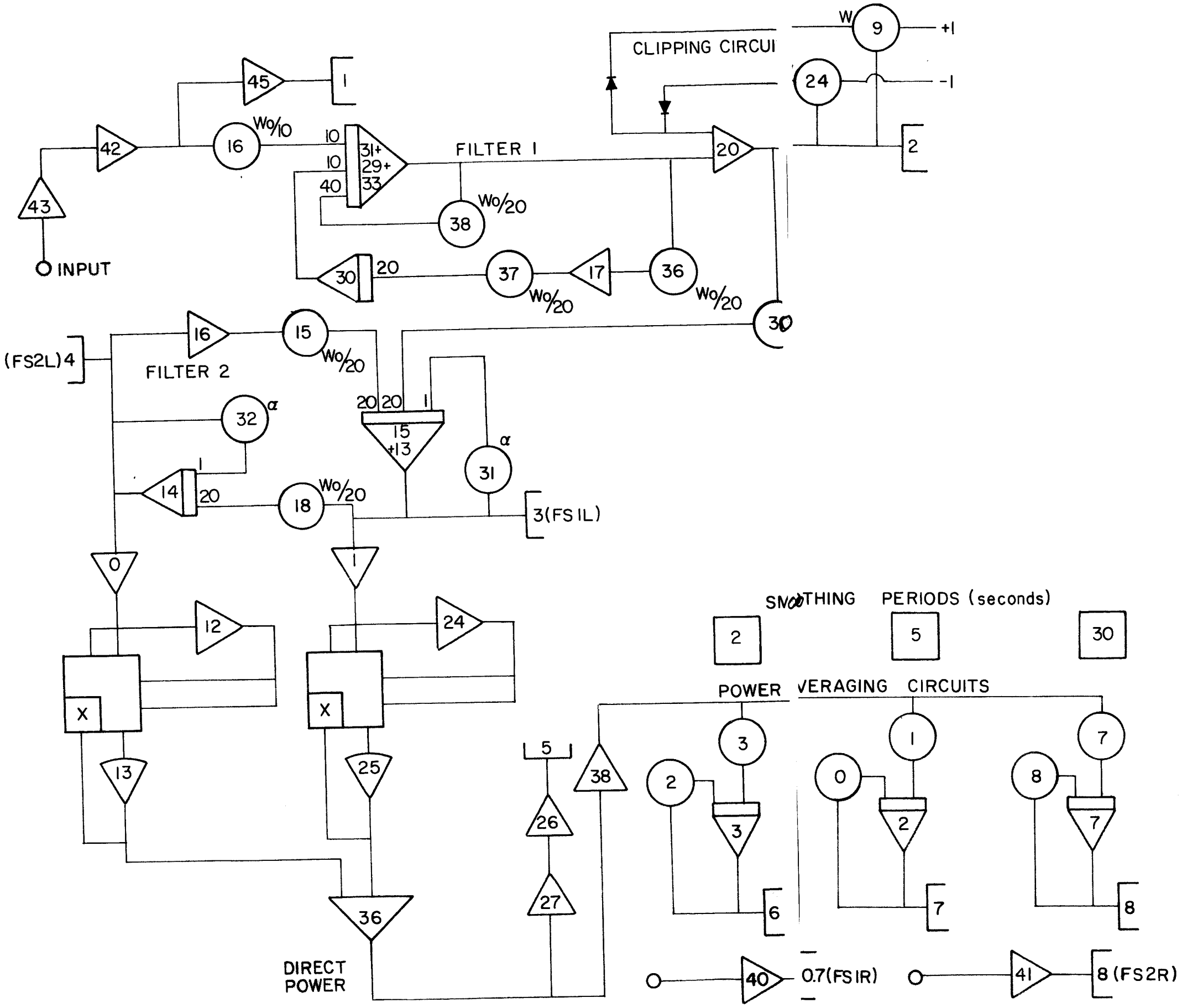

Fig. E6. Block Diagram of Analog Filters for Finding E(f) and G(f)

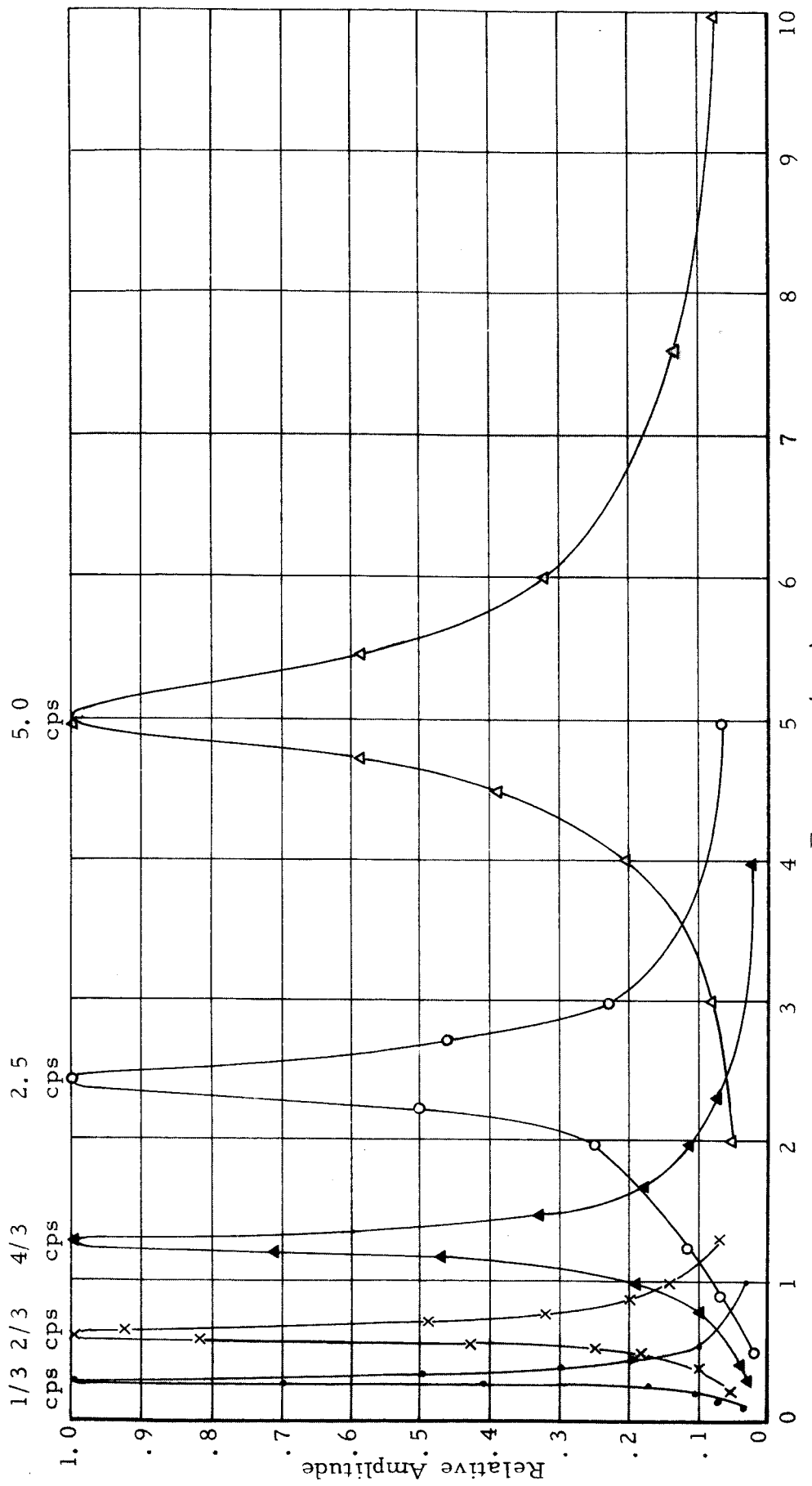

Fig. E7. Typical Filter Characteristics

Fig. E8. Time Histories of u, w, E(f) and G(f), June 18

u and w in Arbitrary Units

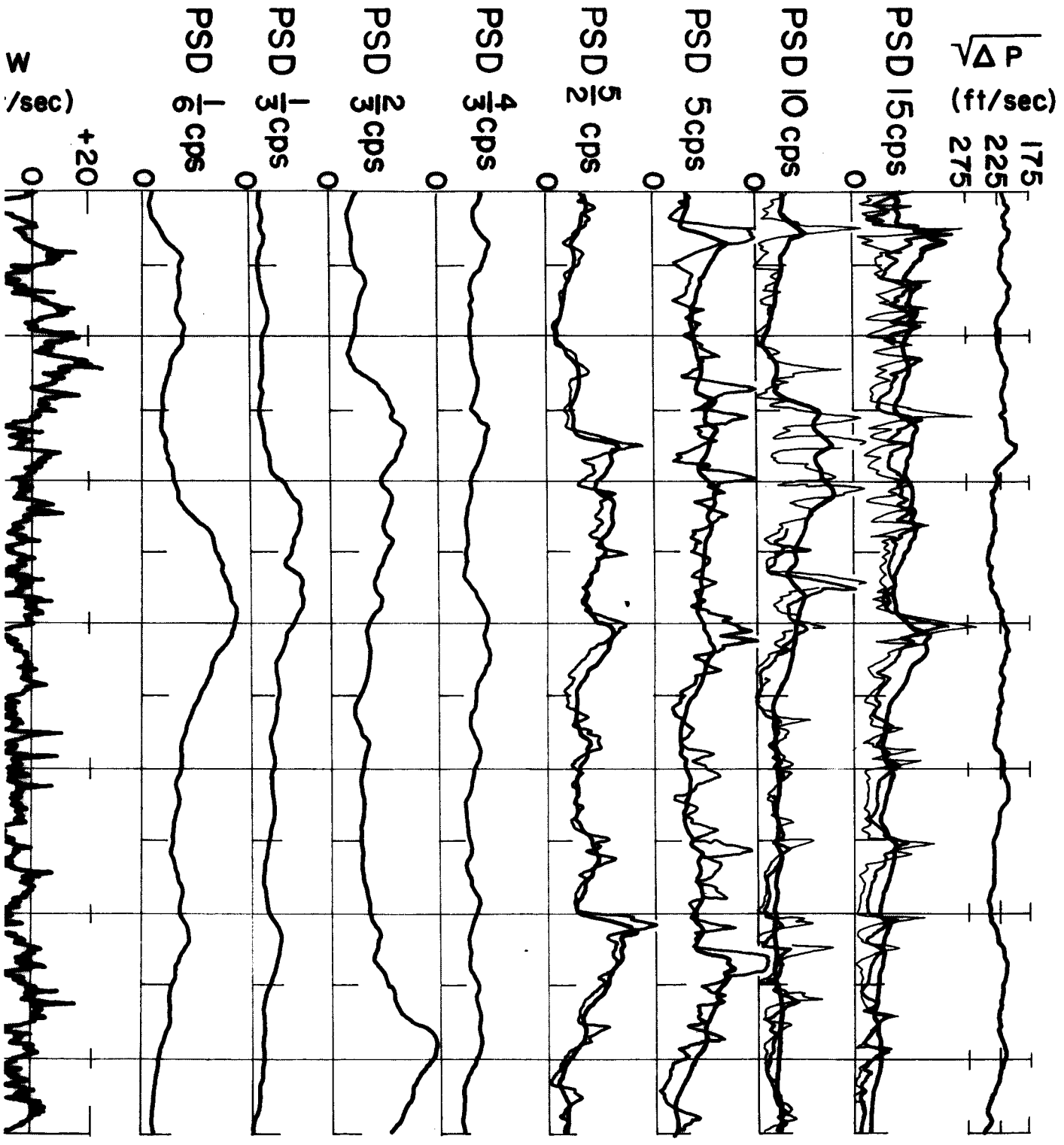

#2

To clarify the matter of time constants further, the magnetic tape recording of Δp for the June 18 case was played into the breadboard version of the UITS, with three separate output channels being recorded simultaneously on a Brush recorder, one with $\tau = 1.8$ sec, one with 4 sec, and one with 12 sec. As a $\tau = 12$ sec was judged too long and for 4 sec a bit short, a reasonable compromise between detailed data and smoothness of data should therefore be in the range of 6 to 10 sec.